Thermophysical Properties of Several Nanofluids as a Function of Temperature and Volume Fraction Developed in Analysis of a Flat-Plate Solar Collector for Performance Improvement

DISSERTATION

THESIS SUBMITTED IN PARTIAL FULFILMENT OF THE REQUIREMENT FOR THE DEGREE OF MASTER OF ENGINEERING IN MECHANICAL ENGINEERING UNDER THE FACULTY OF ENGINEERING AND TECHNOLOGY

By

TANMOY MONDAL

Class Roll Number: 002011202011
Registration No.: 154310 of 2020-21
Exam Roll No.: M4MEC22011
Academic Session: 2020-2022

under the guidance of

PROF. BALARAM KUNDU

Department of Mechanical Engineering
Jadavpur University

JADAVPUR - 700032

DECLARATION OF ORIGINALITY AND COMPLIANCE ACADEMIC ETHICS

I hereby declare that the thesis entitled "**Thermophysical Properties of Several Nanofluids as a Function of Temperature and Volume Fraction Developed in Analysis of a Flat-Plate Solar Collector for Performance Improvement**" contains a literature survey and original research work by the undersigned candidate, as a part of his MASTER OF ENGINEERING IN MECHANICAL ENGINEERING under the DEPARTMENT OF MECHANICAL ENGINEERING, studies during the academic session 2020-2022.

All information in this document has been obtained and presented in accordance with the academic rules and ethical conduct.

I also declare that, as required by these rules of conduct, I have fully cited and referenced all the material and results that are not original to this work.

Name: TANMOY MONDAL

Class Roll Number: 002011202011

University Registration No: 154310 of 2020-21

Examination Roll No: M4MEC22011

Date:

Signature:

FACULTY OF ENGINEERING & TECHNOLOGY

DEPARTMENT OF MECHANICAL ENGINEERING

JADAVPUR UNIVERSITY

KOLKATA-700032

CERTIFICATE OF RECOMMENDATION

This is to certify that the thesis entitled "**Thermophysical Properties of Several Nanofluids as a Function of Temperature and Volume Fraction Developed in Analysis of a Flat-Plate Solar Collector for Performance Improvement**" is a Bonafede work carried out by TANMOY MONDAL under our supervision and guidance in partial fulfillment of the requirements for the degree of Master of Engineering in Mechanical Engineering under the Department of Mechanical Engineering, Jadavpur University, during the academic session, 2020-2022.

Prof. Amit Karmakar
Head of Department
Department of Mechanical Engineering
Jadavpur University, Kolkata

THESIS SUPERVISOR
Prof. Balaram Kundu
Professor
Department of Mechanical Engineering
Jadavpur University, Kolkata

Prof. Chandan Mazumdar
Dean
Faculty Council of Engineering and Technology
Jadavpur University, Kolkata

FACULTY OF ENGINEERING & TECHNOLOGY

DEPARTMENT OF MECHANICAL ENGINEERING

JADAVPUR UNIVERSITY

KOLKATA-700032

CERTIFICATE OF APPROVAL

The foregoing thesis, entitled "**Thermophysical Properties of Several Nanofluids as a Function of Temperature and Volume Fraction Developed in Analysis of a Flat-Plate Solar Collector for Performance Improvement**" is hereby approved as a creditable study in the area of Mechanical Engineering carried out and presented by TANMOY MONDAL in a satisfactory manner to warrant its acceptance as a prerequisite to the degree for which it has been submitted. It is notified to be understood that by this approval, the undersigned does not necessarily endorse or approve any statement made, opinion expressed, and conclusion drawn therein but approves the thesis only for the purpose for which it has been submitted.

Committee of the final evaluation of the thesis:

Signature of Examiners

Abstract

Based on our theoretical findings on varying mass flow rate, temperature, and nanoparticle volumetric fraction, the current analysis focuses on regression model analysis of a wide variety of nanofluids for evaluating thermal properties, performance, and heat transfer of flat plate solar collector in terms of various parameters as well as in respect to energy and exergy efficiency. Theoretically, all nanofluids were sampled at varied nanoparticle volumetric fractions and temperature ranges. To develop a correlation model for the thermal conductivity, specific heat, and viscosity of the nanofluids, their thermal characteristics were tested for various temperature ranges. Results show that heat transfer for magnetic particles in water is higher and enhanced by 89 percent for fixed particle volume concentration, temperature, and mass flow rate, followed by MgO-TiO2/water, clove-treated carbon nanoplatelet/water, Al2O3 Oxide/water, and Al2O3-Fe/water, respectively, in place of water as the base fluid. Reynolds number, a measure of heat resistance, is likewise at its highest for MgO-TiO2/water nanofluids by 31%. Al2O3-Fe/water is followed by Al2O3 Oxide/water, clove-treated carbon nanoplatelet/water, MgO-TiO2/water, and magnetic particle/water in order of the friction factor, which indicates pressure drop in the system, is enhanced by 70%. Magnetic particle/water has the highest absorbed energy parameter. Al2O3-Fe Oxide/water has the highest exergy efficiency, which measures the useable energy, increasing it by 28 percent, followed by other nanofluids. Increased system performance in effectively converting the available energy into functional processes is highlighted by the rise of the Bejan number towards unity.

Acknowledgments

Foremost, I would like to express my sincere gratitude to my advisor **PROF. BALARAN KUNDU** for enlightening me the first glance of research, and for his patience, motivation, enthusiasm, and immense knowledge. His guidance helped me in all the time of research and writing of this thesis. I could not have imagined having a better advisor and mentor for my project work.

The computer support for searching research papers by **DIGITAL LIBRARY MEMBERS** of **CENTRAL LIBRARY,JADAVPUR UNIVERSITY** is thankfully acknowledged.

I am thankful to all my classmates and friends who made my stay in Jadavpur, an unforgettable and rewarding experience.

Finally, I feel great reverence for all my family members and the Almighty, for their blessings and for being a constant source of encouragement.

TANMOY MONDAL

M.E ("Mechanical Engineering")

2nd Year, Final Semester

Department of Mechanical Engineering

Jadavpur University, Kolkata

Contents

List of Figures and Tables

NOMENCLATURE

A : surface area of collector (m^2)

A_s: surface area of edges (m^2)

C: constant defined in equation

C_b :bond conductance(W/mK)

c_p: specific heat capacity (J/kg.K)

D: outer diameter of the tube (m)

D_i: inner diameter of tube (m)

E: exergy (W)

F: standard fin efficiency

F': efficiency factor of collector

F_R: removal heat factor

h: heat transfer coefficient (W/m^2K)

h_f: fluid heat transfer coefficient (W/m^2K)

I: solar radiation on solar plate collector (W/m^2)

k: thermal conductivity (W/m K)

k_b :bond coductivity(W/mK)

K :extinction coefficient

L: length of riser (m)

$\dot{m}$: mass flow rate (kg/s)

n :refractive index

N: glass covers number

Nu: Nusselt number

P: pressure of fluid (Pa)

Pr: Prandtl number

Q: heat flux (W)

Re: Reynolds number

t: thickness (m)

T: temperature (K)

U: heat loss (W/m^2K)

V_w: wind velocity above collector(m/s)

V_b: base fluid volume (l)

W: tube spacing in collector(m)

GREEK SYMBOLS

Δ: drop

β: Tilt angle

Η : efficiency

ρ :density (kg/m^3) , reflectance

τ :transmittance

γ :verage bond thickness

α : absorbance

Ɛ : emissivity

μ : dynamic viscosity (Pa s)

σ :Boltzmann constant

φ :volumetric fraction of nanoparticles

θ :angle(^{0})

SUBSCRIPT

a : absorber plate

bc :bottom

bf :base fluid

b : bond width

d :destroyd

D :diffused radiation

ex :exergy

eff: effective

f :fluid

g :glass cover

hnp :hybrid nanoparticle

l :loss

np: nanoparticles

nnp: number of nanoparticles

nf :nanofluids

n :number of particles

p ;plate

r :riser

s :side

t :top

th :thermal

u :useful

1. INTRODUCTION

Researchers and engineers are developing new technologies and more effective devices to harness energy more effectively. Nanofluids are one such invention that has transformed energy absorption and transportation over the years and storage systems. Several important parameters to consider when it comes to improved thermal performance make significant changes as the size of material changes from macro to nano form. These variables are density, viscosity, specific heat, optical extinction coefficient, and thermal conductivity. A unique type of heat exchanger called a solar collector can partially convert incident sun irradiation into usable heat. Any solar system would be incomplete without a solar collector. In a traditional setting, This device absorbs the incoming heat during the heat transformation process. Solar energy is converted to heat by solar radiation, which is subsequently transferred to heat source fluids (air, oil, water). Around the world, flat plate collectors and evacuated tube plate collectors are used. Collectors (ETCs) are frequently utilized in solar energy absorbing systems. Thanks to years of experience, development, and research, its straightforward design, compactness, cheap production costs, maintenance costs, and long-term dependability. However, efficiency is a factor. Combining traditional solar collectors with conventional heat absorbing sources, the ability to absorb heat in fluids is limited.

1.1 LITERATURE REVIEW

Lee et al. [1] took the properties of nanofluids are dependent on the morphologies of nanoparticles, transmission electron microscopy, and scanning electron microscope images to characterize the form and size of SiC nanoparticles. The zeta potential values were used to characterize the dispersion behavior of SiC/deionized water (DIW) nanofluids at various pH levels. Then, in order to evaluate their potential as more efficient working fluids in heat transfer applications, the viscosity and thermal conductivity of silicon carbide in distilled water nanofluids were studied as a function of volume fraction. Kumaresan et al. [2] research were to test and characterize the thermo-physical properties of CNT nanofluids made from a water–ethylene glycol mixture at different temperatures. The measured densities show a clear deviation from the expectations of the Pak and Cho connection due to the limited spontaneous filling of water inside the carbon nanotubes. The specific heat of nanofluids is markedly increased by the presence of multiwall carbon nanotubes (MWCNT), and it is lowered as MWCNT concentration rises.Nine et al. [3] regulated synthesis of Cu2O and cermets of Cu/Cu2O nanoparticles is achieved by hydrolysis of copper (Cu) particles (200 nm or even microsize) using low-energy ball milling in an aqueous environment. Ground particles in aqueous solution are discovered in nano bar and spherical shapes, with cluster nano-clouds. Cu2O nanoparticles and Cu/Cu2O cermets generated by complete and imperfect oxidation of Cu particles are confirmed by X-ray diffraction patterns of the sample powder. Cu2Oewater and Cu/Cu2Oewater nanofluids have higher thermal conductivity than non-ground Cuewater nanofluids, which are measured and compared. Aravind et al. [4] synthesized Graphene and graphene–multiwalled carbon nanotube (MWNT) composites utilising a solution-free green process based on focused solar electromagnetic radiation. Stable nanofluids are made by dispersing nanomaterials in polar base fluids. The thermal

conductivity of the nanofluids increases with the addition of graphene-MWNT nanocomposites, which may be due to MWNT's ability to prevent the restacking of graphene sheets as well as a synergistic effect of both materials' high intrinsic thermal conductivity. Thermal conductivity is improved by 9.2 % and 10.5 %, respectively, with graphene and graphene-MWNT nanofluids in deionized water at ambient temperature for a 0.04 % volume fraction.Nikkam et al. [5] used Directly forming copper nanoparticles in diethylene glycol with microwave assistance to heat the mixture uniformly, accelerating the nucleation of metal clusters and producing monodispersed nanostructures. The physicochemical parameters of nanofluids, such as thermal conductivity and viscosity, were measured in the temperature range of 20e50 for nanofluids with nanoparticle concentrations ranging from 0.4 wt % to 1.6 wt %. Elias et al. [6] tested Thermal conductivity, viscosity, density, and specific heat at various temperatures (ranging from 10 to 50 °C) and nanoparticle volume concentrations (from 0 to 1 vol. %). The nanofluid's thermal conductivity, viscosity, and density all rose as the volume concentrations increased. However, when the volume concentration of nanoparticles increased, the specific heat of the nanofluid fell. Furthermore, increasing the temperature increased the thermal conductivity and specific heat while decreasing the viscosity and density. Karimi et al. [7] explored the thermal conductivity of magnetic nanofluids (MNFs) containing MFe2O4 (M = Fe and Co) nanoparticles suspended in deionized water, in the presence and absence of a homogenous magnetic field. The co-precipitation process is used to make Fe_3O_4 and $CoFe_2O_4$ nanoparticles. MNFs' thermal conductivity was evaluated at varied volume fractions ranging from 0 to 4.8 % and magnetic field intensities ranging from 0 to 500 G. The experimental results reveal that when the volume fraction and magnetic field intensity increase, the thermal conductivity of MNFs increases until it reaches saturation. Li et al[8] coated SiO_2-coated graphene on the graphene surface utilising a chemical liquid deposition process using tetraethyl orthosilicate (TEOS).

An innovative kind of stable water-based graphene nanofluid was developed using the functionalized nanomaterial (graphene/silicon oxide). A water-based graphene nanofluid's stability and thermal conductivity were examined in relation to the impact of SiO_2-coating. Sundar et al[9] dispersed Magnetic Ni nanoparticles in distilled water to create a magnetic nanofluid. The viscosity and thermal conductivity of the nanofluid were experimentally determined as functions of particle concentration and temperature. Furthermore, the Nusselt number and friction factor were calculated experimentally as a function of particle concentration and Reynolds number for constant particle concentrations.Heat flux in a forced convection system with no phase shift in the nanofluid running through a tube The results show that as the particle volume fraction and Reynolds number increase, so the Nusselt number and friction factor of the nanofluid also increases. Manikandan et al[10] used Extended probe ultrasonication to disperse sand nanoparticles generated by stirred milling in propylene glycol, resulting in stable sand with propylene glycol nanofluids. With the increasing nanoparticle fraction (0–2 vol %) and temperature (29–140^{0}C), the viscosity of sand–propylene nanofluids reduces. The impact of nanoparticle concentration and temperature (10–50°C) on thermal conductivity was investigated, and it was discovered that thermal conductivity increases linearly with nanoparticle concentration. Rakhsha et al[11] studied the steady state turbulent forced convection forming flow of a CuO nano-fluid inside helically coiled tubes at constant wall surface temperature was studied numerically and experimentally in the current study.Huminic et al[12] evaluated FeC/water nanofluids and the effectiveness of temperature and weight concentration on their thermophysical properties. The FeC nanoparticles were made using a laser pyrolysis method. Thermal conductivity, viscosity, and surface tension of FeC/water nanofluids were examined at three weight concentrations in the temperature range of 10 °C to 70 °C (0.1, 0.5 and 1.0 wt %).. Yarmand et al[13] used a simple chemical reaction approach to create a GNP–Ag uniform

nanocomposite, which gives acid treatment for GNP formation. In compared to the base-fluid, the experimental data for GNP–Ag nanofluids showed improvements in effective thermal conductivity and heat transfer efficiency. For a weight concentration of 0.1 % at a Reynolds number of 17,500, the maximum enhancement in Nusselt number was 32.7 % with a penalty of 1.08 times increase in the friction factor compared to pure water. Amiri et al [14] discovered the GNP-COOH/water nanofluids to be particularly effective in the thermosyphon in terms of thermal properties such as net heat transfer, entropy, and thermal efficiency, as well as rheological properties such as effective viscosity, as well as total pressure drop. This is in contrast to GNP-SDBS/water nanofluids and undoubtedly with distilled water. Microwave-assisted covalent functionalization is a quick and cost-effective technology for industrial applications, as well as an environmentally benign alternative to surfactant-based approaches. Solangi et al[15] examined Nanofluids are nanoparticle suspensions in a fluid medium that have improved characteristics at low nanoparticle concentrations. Nanofluids are used in high heat flux systems because of their unique heat transfer capabilities (e.g., cooling systems, heat exchanger , solar collectors). This study discusses the factors that influence nanofluid stability as well as the various methods for assessing nanofluid stability. This work also includes an updated assessment of nanofluid qualities, including as physical and rheological properties, with a focus on the heat transfer increment. Karim et al[16] investigated the thermal conductivity of $NiFe_2O_4$ nanoparticles distributed in distilled water using experimental methods. A microemulsion process is used to make the magnetic nanoparticles. The thermal conductivity of the produced nanofluids is measured experimentally at varied volume concentrations between 0 and 2 % and at temperatures ranging from 25 to 55^0C. The thermal conductivity of nanofluids increases with increasing volume concentration and temperature, according to the findings. Said et al [17]explored The thermo-physical characteristics effects on short Single Wall

Carbon Nanotubes (SWCNTs) suspended in distilled water in this work because to improve the thermal efficiency of a solar collector. The increment of thermal conductivity was related to particle fraction and temperature. The viscosity of nanofluids and water decrease as the temperature rise and increased as particle fraction increased. The energy and exergy efficiency of the flat plate collector were increased to 95.12 % and 26.25 %, respectively, using better thermo-physical properties of the nanofluid, compared to 42.07 % and 8.77 %, respectively, using water. Flat plate collectors still need to be improved because of their low exergy efficiency. Azmi et al[18] conducted The research by measuring the heat transfer coefficient of TiO_2 nanofluids in a circular tube under turbulent flow. Temperatures ranging from 30 to 80^0C were used to measure thermal conductivity and viscosity. At a concentration of 1.5 vol% and a temperature of 60^0C, the highest increase in thermal conductivity was 15.4 %. Temperature causes the relative viscosities to change between 4.6 and 33.3 %. For temperatures of 50^0C and 70^0C, the Nusselt number increased by 22.8 % and 28.9 %, respectively. With increasing concentration, the friction factor for nanofluids increases marginally.Sarsam et al[19] prepared trithanolamine-treated graphene nanoplatelets (TEA-GNPs) with various particular areas is demonstrated using an unique synthetic process (SSAs). The covalently functionalizedTEA-GNPs with various weight concentrations and SSAs were dispersed in distilled water using ultrasonication to createTEA-GNPs nanofluids. To make stable water-based nanofluids, a simple direct connection of GNPs with TEA molecules is used. Water in base TEA-GNPs nanofluids exhibited Newtonian behaviour, as observed viscosity values increasing as weight concentration and temperature decreased. Maheswaran et al[20] investigated dispersion and thermal stability of garnet-lubricant oil nano fluids using a typical two-step approach. The gravity driven sedimentation test is used to find the stability of nanofluids, while Thermo Gravimetric Analysis (TGA) techniques are used to find the thermal stability. The results reveal that the generated nano fluids are

extremely stable up to 500 °C, and that the viscous behaviour is strengthened as nano particle concentrations increase. Shanbedi et al [21]functionalized MWNT with aspartic acids, a connection of carboxylic acid-treated multi-walled carbon nanotubes (MWNT) surface with amines are used (Asp). Fe ions covalently connected with the carboxylic acids group of Asp to impart magnetic properties to the surface of MWNT. The ferromagnetic MWNT-based in water nanofluids were generated at varied fractions to evaluate the thermo-physical and rheological properties in the second part of the investigation. The behaviour of MWNT-based water nanofluids in terms of density, viscosity, electrical, and thermal conductivity of ferromagnetic (Fe), covalent (Asp), and non-covalent (Gum Arabic) functional groups was examined, with promising results. When compared to covalent nanofluids, the rheological and thermophysical parameters of ferromagnetic samples were dramatically improved. Li et al[22] presented datas on the thermal conductivity and viscosity properties of DO-based SiC nanofluids in order to address a research gap in the literature. The thermal conductivity of nanofluids were find to improve with volume fraction, with the maximum thermal conductivity enhancement of 7.36 % for 0.8 vol. % nanofluid at 50^0C. The produced DO/SiC nanofluids exhibited Newtonian behaviour, with viscosities decreasing as temperature increased. Furthermore, as the temperature rose, the overall effectiveness of nanofluids dropped, indicating that they might be used in high-temperature energy systems. Li et al[23] presented fresh discoveries on the viscosity, thermal conductivity of silicon carbide (SiC) nanofluid-based vehicle engine coolants. The two-step approach with the inclusion of surfactant produced homogeneous and stable nanofluids with volume fractions up to 0.5 vol. % (oleic acid). The nanofluids thermal conductivity improved with volume fraction and temperature (10–50 °C), with the thermal conductivity enhancement recorded for 0.5 vol. % nanofluid at 50 °C at 53.81 %. Furthermore, the overall effectiveness (0.2 vol. %) of the current nanofluids was found to be 1.6, indicating that the car engine coolant-based SiC

nanofluid prepared in this work was superior to the car engine coolant employed as the base liquid in this investigation. Yarmand et al[24] studied, a synthesis approach for the decorating of platinum (Pt) on functionalized graphene nanoplatelets (GNP) was introduced, as well as the production method for nanofluids. A simple chemical reaction technique that included acid treatment for GNP functionalization resulted in a GNP–Pt uniform nanocomposite. Different instruments were used to examine the effective thermal conductivity, density, viscosity, specific heat capacity, and stability of functionalized GNP–Pt water based nanofluids. The GNP–Pt hybrid nanofluids were made by dispersing the nanocomposite in a base fluid without the need of a surfactant. Wan et al [25]used The sono-chemical approach to create epoxy-based all polymer nanocomposites reinforced with Polyaniline (PANI) nanofibers. Ultrasonic velocity, attenuation, and thermal conductivity in PANI-Epoxy nanocomposites were investigated in a wide temperature range (298e373 K) at varied PANI nanofiber loadings (1 & 2 wt %). Existing phenomena are used to describe the behaviour of thermal conductivity and ultrasonic attenuation in synthesised nanocomposites as function of temperature. Esfe et al[26] investigated The viscosity of MWCNTs/ZnO-SAE40 hybrid nano-lubricants at various temperatures and volume fractions. The nano-lubricant acts like a Newtonian fluid, according to the findings. Viscosity experiments also revealed that viscosity reduces as temperature rises and increases when the solid volume %age rises. Gómez et al[27] improved the thermophysical properties of the Heat Transfer Fluids (HTF) utilised in Concentrated Solar Power (CSP) technology . Nanofluids were created by adding Ag nanoparticles to a base fluid made up of a eutectic mixture of diphenyl oxide and biphenyl. When compared to the base fluid, the nanofluids had better thermal properties, with the heat transfer coefficient improving by up to 6%. To gain a better understanding of the nanofluid system at a molecular level, molecular dynamic computations were used. Verma et al[28] investigated a many others types of nanofluids for evaluating flat

plate solar collector performance in terms of a variety of parameters, including energy and exergyefficiency.In addition, the current inquiry was conducted with the optimal particle volu me concentration, based our experimental findings on altering mass flow rate. Entropy forma tion is minimal in Multiwall carbon nanotubebasedwater nanofluids, which is a disadvantage. As the Bejan number approaches u nity, it indicates that the system is doing better in terms of converting available energy into us eful functions. Multiwalled carbon nanotube/water has the biggest increase in energy efficien cy of a collector, at 23.47 %, followed by 16.97 %, 12.64 %, 8.28 %, 5.09 %, and 4.08 % for graphene/water, Copper oxide, Aluminum oxide , and graphene in water, respectively. Multiwalled carbon nanotube/water has the highest increase in energy efficiency of collector, at 23.47 %, followed by 16.97 %, 12.64 %, 8.28 %, 5.09 %, and 4.08 % for graphene/water, Copper oxide in water, Aluminum oxide in water, Titanium oxide in water, and Silicon oxide/water, respectively, using water as base fluid. Zhang et al[29] produced Controlled reduced graphene oxide (CRGO) in this study using modified Hummers' and chemical reduction processes. Without the use of any surfactants, deionized water-based nanofluids of various concentrations were generated using an ultrasonic probe. Furthermore, employing various experimental approaches, the stability, potential, thermal conductivity, rheological features of the prepared nanofluids were extensively studied. Thermal conductivity increases significantly with increasing additive fraction and nanofluid temperature when compared to base fluids, reaching a high of 32.19 % at 60 ^{0}C for a concentration of 1.0 mg/ml. Huminic et al[30] studied is to fabricate, characterise, and prepare water based on SiC nanofluids, as well as to investigate their properties experimentally. Thermal conductivity, viscosity, surface tension of SiC/water nanofluids were measured at temperatures ranging from 20 to 50 degrees Celsius for two weight concentrations of nanoparticles, 0.5 and 1.0 wt %, respectively. The thermal conductivity of the examined nanofluids rises with increasing both

the weight concentration of the nanoparticles and the temperature, according to the experimental data. Furthermore, the dynamic viscosity of SiC/water nanofluids rises with increasing nanoparticle concentration and falls with rising temperature. Furthermore, when the weight concentrations of nanoparticles grow, the surface tension of the examined nanofluids increases. Zawawi et al[31]used the Thermal Properties Analyzer and the Rheometer were to measure thermal conductivity ,viscosity, respectively. The thermal conductivity and viscosity of composite nanolubricants rise with volume concentration and decrease with temperature, according to the findings. In the temperature and volume concentration ranges tested, composite nanolubricants behave like Newtonian fluids. For use in refrigeration systems, a new correlation model to predict the properties of composite nanolubricants has been developed. Sadri et al[32] used free radical grafting process to functionalize the MWCNTs in one pot. Raman spectroscopy, X-ray photoelectron spectroscopy, and transmission electron microscopy are used to analyse the CMWCNTs. Zeta potential measurements are used to verify the electrostatic attractions between the CMWCNT particles in DI water. The stability of the CMWCNTs in the base fluid is also tested using UV– spectroscopy. Experimentally, the thermo-physical properties of the CMWCNT nano-fluids are investigated, and this type nano-fluid does indeed display dramatically improved thermo-physical properties, demonstrating its excellent potential for diverse thermal applications. Nimdeo et al[33] studied the temporal sequence of recorded interferograms as well as analytical tests show a significant increase in thermal diffusivity with increasing temperature and concentration of Al_2O_3 nanofluid suspension. Furthermore, measuring the -potential, pH, and effective viscosity of dilute Al_2O_3 solution at various temperatures illustrates the putative microscale mechanisms that are accountable for such an abnormal thermal diffusivity behaviour. The results show that the greater conductivity of solid alumina particles, as well as their cluster formation, play a significant role in improving the

thermophysical properties of the nanofluid Al_2O_3 solution over the temperature and concentration range studied.. Sadri et al[34] created highly stable and ecologically friendly covalently functionalized graphene nanoplatelet (GNP) aqueous solutions for use of coolants in the heat transfer systems. Using the one-pot approach, the GNPs were functionalized with clove buds. To make the CGNP-water nanofluids, we dispersed the CGNPs in distilled water at three different particle concentrations (0.025, 0.075, and 0.1 wt %) (nano-coolants). The thermo-physical properties of CGNPs nanofluids are significantly improved over those of distilled water. In a fully formed turbulent situation, we conducted heat transfer studies for CGNP-water nano-coolants flowing through the horizontal heated tube. Our findings are encouraging, since the Nusselt number and convective heat transfer coefficient for CGNP-water nanofluids have both increased significantly. Sekhar et al[35] introduced to homogenise the fluid, cobalt oxide nanoparticles and decyl glucoside surfactant to de-ionized water , bath sonicated. The thermo-physical parameters of the nanofluid, such as relative viscosity and thermal conductivity, are investigated at different volume fractions of Cobalt oxide nanoparticles ranging from 0.1vol % to 0.4vol % throughout a temperature range of 30^{o}C to 60^{o}C. The results revealed that relative viscosity values decreased with temperature rise and rose with the increasing nanoparticle volume %age. Esfe et al[36] used Cupper-oxide nanoparticles , Multi-Wall Carbon Nanotubes (CuOMWCNT (9:1) were mixed into a commercial oil lubricants (10w40), rheological behaviours were observed. CuO-MWCNT (9:1)-10w40 was found to have non-Newtonian rheological properties, similar to its bare equivalent. The experimental data were first validated using the Ostwald model, and then utilised to create a new model that linked the volume concentration of the solid phase and the temperature to the composite nano-viscosity of fluid's to support the rheological behaviour of synthesised nano-fluids, an artificial network (ANN) based on the multilayer perception (MLP) algorithm was built .Shi et al[37] investigated the effectiveness of a

magnetically controlled heat transfer system . This approach allows for regulated heat exchange in a rectangular container filled with Fe_3O_4@CNT nanofluid. The magnetically controlled heat transfer approach enhanced the thresholds of heat transfer efficiency by enhancing convective heat transfer as compared to traditional natural convective heat transfer. Tadepalli et al [38] studied considers Al_2O_3, TiO_2, SiO_2, SiC, and CuO in 1 % -5 % volumetric composition in a temperature range of 55-90K and a constant pressure of 2bar to characterise thermophysical properties. According to the findings, as temperature rises, viscosity , density, thermal conductivity, decrease. Specific heat, on other hand, will increase significantly when the temperature rises. viscosity , Density, thermal conductivity, rise as the volume concentration of nano particles increases, but specific heat decreases. Yang et al[39] carried out The experiments at temperatures ranging from 25 to 55 °C, with volume fractions ranging from 0.125 to 1.5 %. In order to investigate the surface and atomic structure of nanoparticles, first they were characterised. After confirming the stability of the nano-lubricant, multiple samples were generated based on volume fraction fluctuations, and the thermal conductivity of the nano-lubricant was measured experimentally. By increasing temperature and concentration, the obtained data demonstrated an ascending trend in thermal conductivity. Ranjbarzadeh et al[40] used A two-step process named eco-friendly nanofluid to prepare water/silica nanofluid samples. The nanofluid's stability , thermal conductivity were investigated. The results of the stability tests revealed that the created samples had good nanostructure and are stable over time, even after the six months of its preparation. The samples' thermal conductivity was measured at temperatures varying from the 25 to 55 ^{0}C and volume fractions of 0.1, 0.25, 0.5, 1, 1.5, 2, 2.5, and 3 % solid. It is crucial to synthesise environmentally friendly silicon oxide nanoparticles with a source for nanofluid manufacturing, and this form of nanofluid can use as an environmental friendly alternative fluid with strong heat transfer capacity in thermal systems. Alawi et al[41] showed that

Al_2O_3/r141b nano refrigerant improves density, dynamic viscosity, and thermal conductivity by 11.54 %, 12.63 %, and 28.88 % when compared to a base refrigerant with the same volumetric fraction and temperature (4 % and 35°c). In comparison to r-141b, Al_2O_3/r141b nano refrigerant has the most notable cop of 2.65 %, 15.13 %, and 3.3 % for specific heat capacity, thermal conductivity, and density. The use of nanoparticles in refrigeration and air conditioning has potential to the improvement of efficiency of these systems. Sulgani et al[42] investigated At varied mass fractions (0, 0.25, 0.5, 1, 2, and 4) the influence of nanoparticle concentration. Experiments were carried out at temperatures varying from 25 to 65 °C, with the results indicating that even the smallest mass concentration improved the nano-thermal lubricant's characteristics. As a result, the most significant improves occurre at a volumes fraction of 4%, or 33% of the base oil. The curve fitting method applied to the data find by experiment to develop a highly precise experimental connection in SigmaPlot to compute the thermal conductivity of the nano-lubricants by using the temperature and volume fractions of the particles. Logesh et al[43] synthesiseed thermophysical property characterization of Aluminum Oxide mixed with ethelene glycol nanofluid with various carbon nanotube concentrations and temperatures are described. In heat transfer applications, the importance of Al_2O_3 nanofluids using EG/water as a base fluid is highlighted. Ghaffarkhah et al[44] examined Four different hybrid nano-lubricants' dynamic viscosity . SAE 40 engine oil was used as the base fluid. COOH-Functionalized MWCNTs made up 20% of the suspended nanoparticles, whereas oxide nanoparticles made up the other 80%. (SiO_2, Al_2O_3, MgO, and ZnO). The trials were carried out at temperatures ranging from 25 to 50 degrees Fahrenheit with solid volumetric fractions of 0.05, 0.25, 0.50, 0.75, and 1%. The viscosity of produced nanofluids was also predicted using decision trees, random forests, Support Vector Machines (SVM), and Radial Basis Function Artificial Neural Networks (RBF-ANN). Karami et al[45] improved this quality, functionalization, a frequent strategy

suggested by many researchers, can be used. In order to prepare homogeneous samples of 0.1 and 0.2 weight %, nanofluids containing graphene nanoplatelets and carboxylated multiwalled carbon nanotube were generated and dispersed in deionized water. For the first time, the effects of ultrasonic time and microwave irradiation on sample stability were examined. Shear stress, viscosity, surface tension, density, and stability were among the thermophysical parameters studied and reported. Yadav et al[46] were devoted to improving the heat transfer performance of Nano fluids used as coolants. There is a pressing need for a multi-lateral analysis of the impacts of introducing nanoparticles into the base fluids. Although the goal of adding nanoparticles is to improve thermal properties, it's also important to consider the impact of this addition on base fluids. The effects of particle volumetric fraction and temperature on viscosity have researched, as well as relative thermal conductivity and relative viscosity. Mahyari et al[47] explored The thermal conductivity of water/graphene oxide-silicon carbide nanofluid experimentally, including the manufacturing process, stability, measurement, and modelling. The measurement of thermal conductivity of hybris nanofluids done at temperatures ranges from 25 to 50 degrees Celsius and volume concentrations ranges from 0.05 to 1 volume %, respectively. With increasing volume fraction and temperature, the thermal conductivity of the nanofluid increased. Changes in thermal conductivity are stronger at high temperatures, despite the fact that nanoparticle volumetric fraction has a greater effect than temperature. Using the laboratory data curve fitting method, a very accurate experimental equation was created to find out the thermal conductivity of nanofluid.. Huminic et al[48] used XDR and TEM techniques to manufacture and analyse La_2O_3 nanoparticles. The generated aqueous nanofluids' thermal conductivity and viscosity were studied at temperatures ranging from 20 to 50 degrees Celsius for three mass concentrations of nanoparticles: 0.5 %, 2.0 %, and 3.0 %. Based on the experimental data, correlations for both heat conductivity and viscosity were proposed. In

addition, the efficiency of lanthanum oxide was investigated, as well as the effect of nanoparticle mass concentration on heat transfer coefficient and pumping power in both laminar and turbulent regimes. Yang et al[49] prepared stability, and thermal conductivity of Graphene oxide/Water Nano-fluid were all investigated in order to improve the thermal characteristics of water. The Nano-fluid has the maximum stability at optimum pH (pH=8), according to the data. The thermal conductivity of the Nano-fluid increased significantly in the studied range, with a maximum increase of 48.1 %. A new correlational with great accuracy has been proposed using the curve fitting method. Mousavi et al[50] investigated This research presents an experimental examination of the thermophysical characteristics and rheological behaviour of MgO-TiO_2/DW (distilled water) nanofluids with weight % ratios of 50:50, 80:20, 20:80, 60:40, and 40:60. MgO and TiO_2 nanoparticles were suspended in distilled water in the presence of Sodium Dodecyl Sulfate (SDS) as a surfactant to create Dual Hybrid Nanofluids (DHNFs). The thermal conductivity of DHNFs was found to be substantially dependent on solid volume concentration and only rarely increased with increasing temperature. The thermal conductivity increase of DHNFs was determined to be 21.8 % for 80 wt% MgO-20 wt% TiO_2 comparable to 0.3 solid vol % at 60 °C for 80 wt% MgO-20 wt% TiO_2. Three empirical correlations were presented to anticipate the aforementioned qualities of DHNFs, with the calculated findings agreeing well. Moghadam et al[51] experimented is to see how a hybrid use of graphene oxide (GO) and titanium oxide (TiO_2) nanomaterials affects the thermal conductivity of water. The studies were carried out at temperatures ranging from 20 to 50 degrees Celsius for concentrations of 0.05, 0.1, 0.2, 0.4, 0.6, 0.8, and 1 %. Increased temperatures and concentrations of nanomaterials result in higher thermal conductivity, according to the experiments. Liu et al[52] varied morphologies, nanosilica, multiwalled carbon nanotubes, and graphite powder have diverse impacts on guar gum fracturing fluid. Nanomaterials increased the apparent viscosity,

temperature tolerance, elastic modulus, and tensile strength of nano-hybrid guar gum fracturing fluids when compared to same qualities of blank fracturing fluids, according to the findings (without nanomaterials). Distinct nanomaterials had different roles in the network structure of guar gum fracturing fluid, according to microscopic investigation by SEM and TEM. In terms of micro particle size, modified nano-SiO_2 (M-NS) in the fracturing fluid served as a nuclear point and skeleton, enhancing the network structure significantly. Guar gum macromolecular chains and hydroxylated multiwalled carbon nanotubes (MWNTs-OH) were interwoven. Kazemi et al[53] investigated At various pH levels, the stability of silica nanoparticles, graphene in base fluid . The thermal conductivity of three different types of nanofluids, SiO_2/Water, G/Water, and G-SiO_2/Water, was measured at varied volume concerntrations of 0.05–1% and temperatures (T) ranging from 25 to 50 °C. The greatest and smallest thermal conductivity enhancements were assigned to SiO_2/Water, G/water mono-nanofluids, respectively; however, thermal conductivity enhancement between the two values and close to the greater value was attributed to G-SiO_2/water nanofluids. Arya et al[54] carried out A series of tests to see if MgO/water-EG (ethylene glycol) hybrid based nanofluids (NF) could be used in a double-pipe heat exchanger in short HEX.The overall heat transfer coefficient (HTC), the working fluid inlet temperature, the fluid pressure drop (FPD), friction factor (FF), and the hydraulic performance index of the nanofluids were all measured within HEX experimentally. The asymptotic particulate fouling model was used to study and model fouling of nanoparticles (NPs) within the Hex. The creation of a porous particle fouling layer on the inner tube's interior wall results in a thermal resistance named by fouling that changes with time, according to the findings. Wang et al[55] investigated the practical lithium-ion battery pack is required in Thermal management systems (TMSs) applications. For the first time ,here , phase change materials (PCM) nano-emulsions with the improvement of energy storage capacity, outstanding performance of dispersion stability ,

reduced viscosity, and strong reliability of temperature were used for coolants in the high-performance liquid cooling thermal management systems (LCTMSs). To evaluate the thermal management performance of various coolants, the highest temperature (Tmax) and high in temperature difference (DTmax) in a 5S4P battery pack evaluated. Tmax and DTmax fell as flow rate of the coolants increased, the thermal management performance of 10 wt% OP28E nano-emulsion is always superior than water. Hatami et al[56] interfaced Nanotechnologies that span a wide range of disciplines and applications, including internal combustion engines. Recent studies on nano-lubricants are gathered and summarised in primary group applications such as engine oil, gear oil, and nanolubricants for refrigeration systems. The effects of these nano-lubricants on engine wear, cold start damage, energy savings, and other factors are also being explored. Okonkwo et al[57] assessed the collector performance using hybrid nanofluids named alumina-iron/water ,alumina-water, , and water as heat transfer fluids using a parametric study and system optimization for different temperatures, nanoparticle fractions, and mass flow rates. The final results suggest that using alumina-water given concentration 0.1 % increased the collector's thermal efficiency by 2.16 %, when using hybrid nanofluid lowered the collector's thermal performance by 1.79 % when it is compared with water. Although hybrid nanofluid did not provide a good thermal option than that of water, it did provide 6.9% increase in exergetic efficiency compared to 5.7 % for the alumina-water nanofluids.. Wole et al[58] compared actual data to classical models and found that the specific heat model overstated experimentally obtained values while the viscosity model underestimated them. According to the findings, the particle mixture ratio has a substantial impact on the hybrid nanofluids' specific heat and viscosity. By raising the volume concentration, viscosity rises while specific heat falls. Ranjan et al[59] Used the liquid exfoliation approach, the study focuses on the reaction mechanism of magnesium diboride and GO. Because of the linked borohydrides and hydroxyl hydrophilic sites, CBNs

form a stable suspension in water and ethylene glycol. In the visible wavelength range, CBNs nanofluids have strong thermal conductivity but poor light absorption capabilities. When compared to Deionized water and ethylene glycole-based fluids, CBNs-rGO nanofluids demonstrate a 95% reduction in the radiation and a considerable increase of 30% and 20% in thermal conductivity, respectively. Stalin et al[60] adjusted the volume concentration of CeO2/water nanofluids from 0.01 to 0.3 in five distinct ways. EDX is used to determine the elemental composition of cerium oxide nanoparticles. Using a scanning electron microscope, the surface properties of CeO2 nanoparticles are investigated. When compared to CeO2/water nanofluids with 0.01 vol concentration, co-efficient of viscosity, thermal conductivity, and co-efficient of density of CeO2/water nanofluids at a 0.3 vol fractions rose by 1.76 %, 35.97%, and 1.56 %, respectively. Omiddezyani et al[61] treated the produced hybrid material with Gallic acid (GA) as a green agent at room temperature, this study offers a simple technique for synthesising a cobalt ferrite/reduced graphene oxide (CoFe2O4/rGO) nanocomposite with good water dispersibility features. The thermal conductivity ratio of ferrofluid generated by the obtained CoFe2O4/rGO with 0.9 wt. % load of nanoparticles rose to 1.46 at 60 C, according to thermo-physical investigations of nanofluids. At Reynolds number 1713, the nanofluid with the highest load of nanoparticles (0.9 wt%) showed the greatest increase in Nusselt number of 27.8%. Tyagi et al[62] investigated their huge capacity to cover the important energy requirments: low-grade thermal energy and electricity , photovoltaic/thermal (PV/T) systems are known to be the future of renewable energy. This research gives a comprehensive overview of the usage of nanofluids (NF) and nano-enhanced phase change materials (NEPCM) in PV/T systems for thermal energy storage (TES). The impact of nanomaterials on thermo-physical properties like thermal conductivity (k), latent heat, subcooling, phase change duration, phase change temperature, viscosity, and density, as well as thermal cycle stability of phase change materials (PCMs) at various operating

temperatures, is highlighted in this paper.This study is expected to provide additional insight into the foundations and perceptions of PV/T systems, resulting in increased thermal efficiency. This research is expected to provide additional information about the basics and perceptions of PV/T systems, resulting in improved thermal efficiency of nanoparticle-based photovoltaic systems integrated with PCM or NEPCM. Perabathula et al[[63] investigated Nano lubricants have a significant advantage in terms of improving the tribological qualities of refrigeration systems. The goal of this study is to minimise frictional coefficients and specific wear rates in refrigerator compressors by incorporating a reduced grapheneoxide (RGO) based hybrid nanomaterial into the lubricating oil (R134a oil). The RGO was made using a modified hummers process and then impregnated with sulphur to produce sulphur-reduced graphene oxide (SRGO) nanosheets.O'Neill et al[64] investigated Phase change dispersions present as potential heat transfer fluids in cooling applications due to their high thermal storage capacity and the latent heat of phase change of the dispersed phase change material. In addition, issues like stability and supercooling must be addressed. A full analysis of the types of dispersion found in the literature, as well as their thermophysical, heat transport, and rheological properties, is covered in this paper. Shi et al[65] garnered Nanostructured magnetic suspensions have outstanding thermophysical properties, and their industrial applications for heat transfer augmentation and thermal control have a lot of attention. This research intends to develop an artificial network based on datas on viscosityand thermal conductivity , specific heat to forecast the property parameters of magnetic nanofluids. Kana et al[66] improved The thermal conductivity of MoO3–H2O nano-sheets based nano-fluid in this work. A series of 2D type nano-sheets with a basal size varying from 108 200 nm2 to 415 631 nm2 make up the MoO3–H2O based nano-fluid. The nano-sheets are made up of a collection of nano-crystallites (_7 nm) with diverse crystallographic orientations and an average diameter of 15 nm, according to a Higher

Resolution Transmission Electron Microscopy (HRTEM) observation. Li et al[67] investigated Hybrid nanofluids for heat transfer have a promising future. Examining the possibility for hybrid nanofluids to be used in practical applications and the process for enhancing thermophysical properties are two of the main objectives of the current study. This study examined the enhanced heat transfer performance and thermophysical property distribution of silicon carbide-multiwalled carbon nanotubes (MWCNTs) hybrid nanofluids based on ethylene glycol for use as coolant in automobile engine cooling systems. Due to the high thermal conductivity, high temperature stability, and coupling effect of two nano-materials, the analysed hybrid nanofluids' thermal conductivity was visibly boosted and increased as the volume concentration climbed. The heat transfer benefit of the SiC-MWCNTs hybrid nanofluid demonstrated its potential for use in automobile radiator systems. Zainon et al[68] investigated this research is to look into the stability and thermophysical properties of TiO2-SiO2 nanofluids made from green bio-glycol. The hybrid nanofluids were created in this study by dispersing TiO2 and SiO2 nanoparticles (20:80) in water and Bio-glycol (40:60) mixed base fluids at various volume %ages ranging from 0.5 to 3.0%. At 3.0 % volume concentration and 70°C, the thermal conductivity of the green Bio-glycol based TiO2-SiO2 nanofluids was up to 12.52 % greater than the mixture of W/BG. Meanwhile, the green Bio-glycol based TiO2-SiO2 nanofluids have a negligible dynamic viscosity increase with temperature. Nwaokocha et al[69] explored The thermo-convection behaviour of MgO-ZnO nanoparticles dispersed in deionised water (DIW) for concentrations of 0.05 vol % and 0.1 vol % at %age weight ratios (PWRs) of 20:80, 40:60, 60:40, 80:20 (MgO-ZnO) in a square cavity for the first time in this research. The viscosity , thermal conductivity of the binary fluids and DIW were measured through experiment for temperatures under consideration. In the BNFs, temperature gradients of hybrid nanoparticles are found to improve Nuav, hav. Furthermore, the highest levels of improvement were 73 % (Nuav), 76 %

(hav), and 72 % (Qav). The introduction of binary fluids in a cavity improved thermo-convection performance significantly. Singh et al[70] investigated One of the most common energy storage strategies for storing waste heat and surplus energy is phase-changing material-based storage of thermal energy. Doping of nanoparticles can improve the efficiency of the PCM-based energy storage device. The impacts of MgO, Al2O3 and SiO2 nanodoping on thermal efficiency and other thermal behaviour of PCM-based systems were investigated experimentally,numerically in this study. Effects of all nanoparticles on charging rates, discharging rates, heat flux ,time, and overall enthalpy are also investigated. The charge rate of Al2O3, MgO, and SiO2 nanoparticles is shown to be greatly raised by 33.8 %, 34 %, and 40 % for Al2O3, MgO, and SiO2 nanoparticles, respectively. Compared to phase change material, the charging rate of Al2O3, MgO, and SiO2 NEPCMs is raised by 33.8 %, 33.8 %, and 41 %, respectively, due to the inclusion of nanoparticles. The discharge rate of Al2O3, MgO, and SiO2-based NEPCMs is also raised by 19.6 %, 25%, and 30%, respectively. The addition of nanoparticles, reduces the control volume while increasing the dynamic viscosity. Lu et al[71] used the phase change material (PCM) for latent heat thermal energy storage (LHTES) is the most effective methods to store and use solar energy. However, the poor thermal conductivity of PCMs has a significant impact on its thermal performance. To improve the thermal conductivity of PCMs, paraffin/nano-Fe3O4 composite PCMs were synthesised in this study, and the preparation procedure was refined. The thermophysical properties of composite PCMs were thoroughly investigated, and the improvements in charging and discharging performance were quantitatively evaluated. Ismail et al[72] Used a two-step technique, hybrid nanolubricant is made by dispersing SiO2-TiO2 nanoparticles in a 50:50 composition ratio into the polyvinyl ether (PVE) compressor lubricant. The experiment was carried out at volume concentrations ranging from 0.01 to 0.10 % at temperatures ranging from 303 to 353 K. The nanolubricant's Newtonian behaviour was

determined, and its relative thermo-physical augmentation was calculated by comparing its performance to that of a pure lubricant. Overall, increasing concentrations increases both rheological and thermal properties, but the same attributes decrease with rising temperature. New regression models for thermo-physical parameters were proposed, with R-squared values of 0.9989 , 0.9920 for viscosity , heat conductivity, respectively, indicating great accuracy.

1.2 DRAWBACK IN PREVIOUS WORK

According to a survey of the literature, researchers have mostly focused on one or two particular nanofluids that have improved thermal conductivity and heat transfer coefficient, and here hasn't been much consistency in the methods used or the findings. A wider spectrum of nanofluids and their volumetric concentrations, mass flow rates require more thorough testing and analysis.

1.3 PRESENT STUDY

The thermal performance of a flat plate collector using Al2O3-water, MgO/TiO2-water, magnetic nanoparticle (Ni, Fe3O4)-water, clove treated graphene nanoplatelet (cgnp)-water, and Al2O3/Fe-water nanofluids are evaluated in this study. Thermal property models are proposed and utilized to theoretically forecast the performance of all the nanofluids in the solar collector based on numerical data derived from a polynomial regression analysis. The entropy and heat transfer coefficient, efficiency, exergy related performance of nanofluids in solar flat plate collector is evaluated using a parametric analysis at different temperatures, volumetric %age of nanoparticles, and with the increase in mass flow rates of nanofluids.

2. Nanofluids' thermophysical properties' regression model constants

Nanofluids are more thermally efficient than other common base fluids. Many researchers hypothesized that the fluids would be useful in a variety of engineering sectors. Accurately determining the thermophysical characteristics of nanofluids in a real-world setting is difficult due to a large number of dependent variables. In addition, various experimental studies are necessary to determine the characteristics of nanofluids. In this portion, thermal conductivity, specific heat capacity, density, and dynamic viscosity of all nanofluids are calculated accurately by using Polynomial Regression methods. The input predictor variables used in this model are temperature and volume fraction of the nanoparticles. Thirty-three experimental data sets are taken from research papers to calculate the properties. The effectiveness of the dependent variables (ratio of thermophysical property values collected by experiments to the base fluid property value) in predicting the independent variables (temperature and nanofluids volumetric fraction) are extensively studied and found that the temperature is the crucial factor in enhancing the thermal properties. The proposed calculations are performed by using MATLAB and EXCEL software. It is observed that an optimized Polynomial regression method shows an accurate agreement with experimental data with Standard error 0.001975, P-Value in between 0 to 0.15, Multiple regression value 0.998, Regression square value 0.996, Adjusted regression square value 0.995; nearer to one; hence the predicted results are reliable shown in the table below.

TABLE 1. REGRESSION MODEL CONSTANTS

AUTHOR	LIMITATIONS	NANO FLUIDS	THERMAL PROPERTY	REGRESSION CONSTANTS a_0	a_1	a_2	a_3	a_4
Mousavi et al[50]	$10℃ \leq T \leq 70℃$ and $0.001 \leq \emptyset \leq 0.005$	Hybrid magnesium oxide-titanium oxide in water	K	0.944205	0.003011	-0.000029	31.87665	1819.797
			μ	0.290433	0.008206	0.000098	-21.4733	11926.04
			Cp	0.999944	-0.000025	0.0000006	-2.47987	58.32673
			ρ	1.001101	0.00000357	0	1.537174	108.6821
Shi et al[37]	$15℃ \leq T \leq 65℃$ and $0.002 \leq \emptyset \leq 0.006$	Magnetic nano particle(Ni, Fe3O4, Co3O4) in water	μ	0.65901	0.010016	-0.00016	35.29375	3382.672
			K	0.875434	0.00637	-0.000046	76.55851	-6341.061
			Cp	1.006208	0.000534	-0.0000048	-2.39885	-1.05805
Okonkwo et al[57]	$20℃ \leq T \leq 70℃$ and $0.0005 \leq \emptyset \leq 0.002$	Aluminium oxide in water	K	1.06333	-0.00311	0.0000588	-7.45244	17797.33
			Cp	0.85630	0.0000699	0.0000015	-30.6928	-16661.1
			μ	1.09721	-0.00462	0.0000303	285.1626	-53506.26
Sadri et al[34]	$15℃ \leq T \leq 50℃$ and $0.00025 \leq \emptyset \leq 0.001$	Clove treated graphene nanoplatelet(cgnp) in water	Cp	0.981968	0.000302	-0.000002	-8.48353	-4244.83
			μ	1.099703	-0.00222	0.0000317	-31.3761	81080.4
			K	0.941766	0.001219	0.00003	72.35941	85384.5
Okonkwo et al[57]	$20℃ \leq T \leq 70℃$ and $0.0005 \leq \emptyset \leq 0.002$	Hybrid Aluminium oxide-Fe in water	K	1.030067	-0.00375	0.00005	130.6383	-22138.63
			Cp	0.764603	0.000814	-0.000001	-264.762	69980.29
			μ	1.69324	-0.02428	0.000215	275.2056	-48992.7
Amiri et al [14]	$10℃ \leq T \leq 90℃$ and $0.00025 \leq \emptyset \leq 0.002$	Gnp (graphene nano platelet)-cooh in water	ρ	1.002435	-0.00032	0.00000449	1.340025	0
			K	0.924779	0.003678	-0.0000064	214.5962	-49148.82
			μ	0.766413	0.010685	-0.0001	494.6736	-175552
Yarmand et al[13]	$15℃ \leq T \leq 45℃$ and $0.0002 \leq \emptyset \leq 0.001$	Hybrid graphene nano platelet-silver in water	K	1.136032	-0.01403	0.000286	126.8221	67470.54
			μ	1.215876	-0.01227	0.00028	215.0766	-14460.56
			ρ	0.999619	-0.000008	0.00000016	1.15156	33.91723
. Yarmand et al[24]	$15℃ \leq T \leq 45℃$ and $0.0002 \leq \emptyset \leq 0.001$	Hybrid graphene nano platelet-platinum in water	K	1.059222	-0.00652	0.000144	53.34285	102797.6
			μ	0.922327	0.009104	-0.000051	255,9117	-51638.47
			ρ	0.999736	0.0000198	-0.0000002	0.723314	37.67885
Shanbedi et al**[21]**	$10℃ \leq T \leq 90℃$ and $0.0005 \leq \emptyset \leq 0.002$	Mwnt(multi wall carbon nanotube) in water-CARBOXIL-ATED MWNT	K	0.74271	0.00339	-0.000016	422.7653	-132750
			μ	1.272899	-0.01104	0.000118	583.4941	-178880
			ρ	0.995468	-0.000055	0.0000036	17.1977	-5103.57
		Mwnt(multi wall carbon nanotube) in water-ASPARTIC ACID	K	0.751544	0.003643	-0.000018	423.2055	-123586
			μ	1.059456	-0.00271	0.0000323	310.6241	-71028.8
			ρ	1.008692	-0.00033	0.0000052	3.28742	-102.92

		TREATED MWNT				6	7	
		Mwnt(multi wall carbon nanotube) in water-Fe TREATED MWNT	K	0.738295	0.005887	-0.000033	357.4971	-92157.2
			μ	1.001042	-0.00093	0.0000163	315.1757	-62794.1
			ρ	1.00767	-0.0002	0.00000491	7.403673	-1804.04
Said et al [17]	$30℃ \leq T \leq 55℃$ and $0.001 \leq \emptyset \leq 0.003$	Swcnt(single walled carbon nano tube)-sds(Sodium dodecyl sulphate) in water	K	0.629912	0.00832	0.000188	94.69028	0
			μ	0.494757	0.026824	-0.00028	141.3464	0
Sarsam et al[19]	$20℃ \leq T \leq 40℃$ and $0.00025 \leq \emptyset \leq 0.001$	Triethanolamine – treated graphene nano platelets (TEA-GNPs) in water	K	1.117785	-0.0101	0.000221	117.7837	5224.495
			μ	0.774825	0.012957	-0.00017	224.7223	-9874.9
Wole et al[58]	$20℃ \leq T \leq 70℃$ and $0.0033 \leq \emptyset \leq 0.0167$	Hybrid aluminium oxide-zinc oxide in water	Cp	0.800124	0.003899	-0.000031	-3.14674	-8.60225
			μ	22.73338	-0.56194	0.003622	-11.0485	18216.02
Sekhar et al[35]	$30℃ \leq T \leq 60℃$ and $0.001 \leq \emptyset \leq 0.004$	Cobalt oxide in water	ρ	1.011198	0.001503	-0.000039	108.4774	-17576.6
			μ	1.137789	-0.00598	0.000452	18.79765	7126.861
Huminic et al[48]	$10℃ \leq T \leq 70℃$ and $0.000 < \emptyset \leq 0.0125$	Fec in water	K	0.929488	0.00317	-0.00002	44.35815	-2518.4
			μ	0.904956	0.0046	-0.000064	72.9002	-4123.87
Amiri et al [14]	$10℃ \leq T \leq 90℃$ and $0.00025 \leq \emptyset \leq 0.002$	Gnp(graphene nano platelet)-sdbs(sodium dodecyl benzene sulphonate (SDBS)) in water	μ	0.508977	0.015888	-0.00007	1505.512	-598077
			K	0.900267	0.002976	-0.00002	273.0595	-135028
Huminic et al[30]	$20℃ \leq T \leq 50℃$ and $0.000 < \emptyset \leq 0.03$	Lanthanum oxide in water	K	0.780215	0.006679	-0.000076	88.24159	-10395
			μ	1.138807	0.008528	-0.00014	67.27993	-7250.8
Wang et al[55]	$20℃ \leq T \leq 50℃$ and $0.1 \leq \emptyset \leq 0.2$	Nano emulsion in water	ρ	1.004843	-0.00023	0.00000322	-0.22233	0
			μ	0.065388	0.004977	-0.00021	19.19859	0
Zhang et al[29]	$20℃ \leq T \leq 60℃$ and $0.002 \leq \emptyset \leq 0.01$	Crgo(controlled reduced graphene oxide) in water	K	0.938738	0.002003	0.00000923	8.199218	1152.453
			μ	3.313341	-0.13948	0.001378	258.5881	11353.71

Karimi et al[7]	$10℃ \leq T \leq 70℃$ and $0.005 \leq \emptyset \leq 0.048$	Magnetic CoFe2O4 (cobalt ferrite) in water	K	0.936416	0.002819	-0.0000048	6.161652	-56.6058
Shi et al[37]	$10℃ \leq T \leq 70℃$ and $0.005 \leq \emptyset \leq 0.048$	Magnetic Fe3O4 in water	K	0.918144	0.003903	-0.000018	5.62788	-51.2866
Karim et al[16]	$10℃ \leq T \leq 90℃$ and $0.001 \leq \emptyset \leq 0.002$	Mwcnt (multi walled carbon nano tube)-cooh in water	ρ	1.009644	-0.00069	0.00000791	3.306301	0
Mahyari et al[47]	$25℃ \leq T \leq 50℃$ and $0.000 < \emptyset \leq 0.01$	Hybrid Graphene oxide-silicon carbide in water	K	0.965885	-0.00092	0.0000643	11.64832	1028.266
Aravind et al[4]	$15℃ \leq T \leq 65℃$ and $0.000 < \emptyset \leq 0.015$	Graphene oxide in water	K	0.930185	0.001576	0.000017	31.60959	-642.103
Kazemi et al[53]	$25℃ \leq T \leq 50℃$ and $0.000 < \emptyset \leq 0.01$	Hybrid graphene-silica (SiO_2) in water	K	0.817343	0.007112	-0.000054	48.09916	-1739.71
Li et al[8]	$25℃ \leq T \leq 50℃$ and $0.00011 \leq \emptyset \leq 0.0004$	Synthesized graphene in water	K	1.040569	-0.01222	0.000336	-263.255	3505211
	$25℃ \leq T \leq 50℃$ and $0.00011 \leq \emptyset \leq 0.0004$	Synthesized graphene-mwnt(multiwall carbon nanotube) in water	K	1.039122	-0.00726	0.000238	-982.109	4597213
Karami et al[45]	$15℃ \leq T \leq 65℃$ and $0.0025 \leq \emptyset \leq 0.02$	Nickel ferrite in water	K	0.981738	-0.000075	0.0000148	12.3977	-249.407
Lee et al [1],	$30℃ \leq T \leq 70℃$ and $0.00001 \leq \emptyset \leq 0.03$	Sic(silicon carbide) in water	μ	0.710224	0.01839	-0.00019	37.70586	-465.68
	$25℃ \leq T \leq 55℃$ and $0.001 \leq \emptyset \leq 0.03$	Silica in water	K	0.914558	0.00017	0.0000548	8.078725	-14.8297
Ranjbarzadeh et al[40]	$10℃ \leq T \leq 77℃$ and $0.001 \leq \emptyset \leq 0.003$	Swcnt(single walled carbon nano tube) in water	Cp	1.080268	-0.00363	0.00004	-30.1163	0

Said et al [17]	$20℃ \leq T \leq 60℃$ and $0 < \emptyset \leq 0.0035$	Magnetic Fe3O4 + cnt(carbon nano tube) nano composites in water	K	1.03459	-0.00223	0.0000235	26.63348	-5220.47
Moghadam et al[51]	$20℃ \leq T \leq 50℃$ and $0 < \emptyset \leq 0.001$	Hybrid nanofluid of graphene oxide-titanium oxide in water	K	0.943143	0	0.0000443	340.0721	-113816
Stalin et al[60]	$20℃ \leq T \leq 60℃$ and $0.0001 \leq \emptyset \leq 0.001$	Cerium oxide in water	K	1.004017	-0.00109	0.0000272	270.6573	-66016.3

3. SYSTEM DESCRIPTION

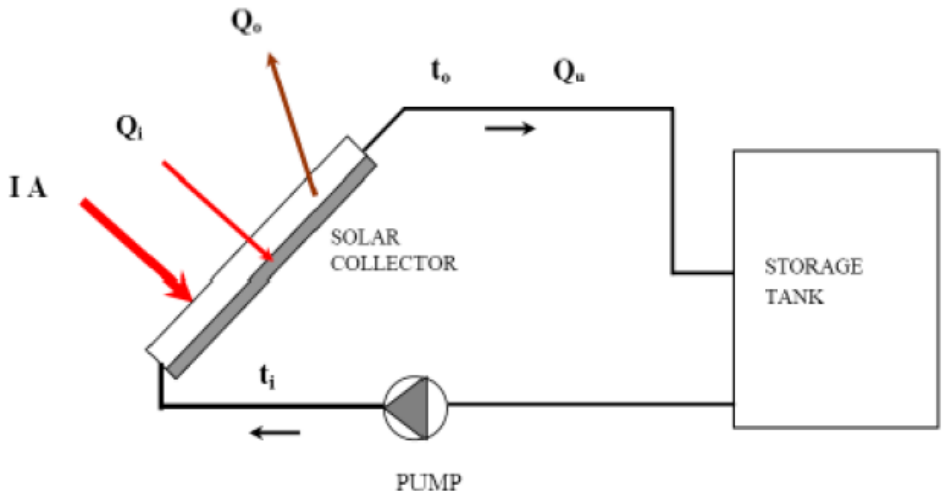

FIG 1 solar energy collection system

The most basic and extensively researched technology for solar-powered household hot water systems is likely flat-plate solar collectors , a mom concentric collector. The general concept of this technology is quite straightforward. The Sun heats a flat, dark surface, which absorbs as much of the energy as it can before transferring it to water for later use. The basic elements of a conventional flat-plate solar collector are as follows: black Surface that absorbs incident solar energy , a translucent coating known as a glazing cover transmits radiation to the absorber but blocks the surface's radiative and convective heat loss. , tubes containing a fluid that heats up to transfer heat from the collector , support system to hold the parts in place and protect them , reduce heat losses by insulating the collector's sides and bottom. Sun's rays travel through transparent cover and strike darkened absorbing surface, which has an high absorption rate. Absorbent plate is made to absorb the high amount of solar light as feasible. The temperature range between 30 and 80 ºC is where flat-plate systems typically function and achieve their highest levels of efficiency.By constraining stagnant air that lies in

between absorber plate and glass cover, transparent cover lowers convection heat losses from the absorber plate caused by the wind. It also aids in lowering the collector's radiative heat losses by making it difficult for the absorber plate's long-wave thermal radiation to escape[73]. Thermal insulators on bottom and sides of absorber plate serve to reduce conductivity losses. The heat transfer fluid using inside the risers absorbs a considerable %age of the thermal energy received by the collector plate[74]. FIG 1 shows the diagram of the Flat Plate Collector(FPC). The dimensions and parameters of the FPC are listed below in TABLE 2.

TABLE 2: Specifications for the solar collector

Flat plate solar collector	Specification
Area of collection (A)	2 m^2
Absorbance(α)	0.90
Extinction coefficient of glass (K)	16.1m^{-1}
Thickness of glass cover(t_g)	0.0023m
Transmittance (τ) at 50^0	0.75
Transmittance (τ) at 70^0	0.54
Incident angle (θ_1)	70^0
Refraction angle (θ_2)	38^0
Refractive index (n_1) of air	1
Refractive index (n_2) of glass	1.526
Transmittance if absorber plate (τ_a)	0.95
Reflectance of diffused radiation (ρ_D)	0.41
Average transmittance absorbance product $(\tau\alpha)_{avg}$	0.70

Number of glass cover on collector (N)	3
Distance in between risers (W)	0.25 m
Thickness of absorber (t_p)	0.004 m
Riser diameter (D)	0.0080 m
Inner diameter of raiser (D_i)	0.0050 m
Riser Length (L)	2.5 m
Emissivity of absorber plate, (ε_p)	0.92
Emissivity of covers, (ε_c)	0.88
Thickness of the insulation (t_i)	0.06 m
Tilt Angle (β)	50^0
Back insulation, thickness (t_b)	0.08 m
Sides' insulation thickness, (t_s)	0.04 m
Thermal conductivity of absorber plate, (K_p)	400 W/m K
Thermal conductivity of insulation, (K_i)	0.04 W/m K
Wind speed above collector (V_w)	1.5 m/s
Ambient temperature (T_0)	288 K
Incident solar radiation on collector surface(I)	1000 W/m^2
Bond conductance (C_b)	∞ W/mK
Pressure drop(ΔP)	500 Pa
Temperature of sun(T_{sun})	5800 K

4. THERMOPHYSICAL PROPERTIES OF NANOFLUIDS

Water values are similar to those of the American Society of Heating, Refrigeration, and air conditioning Engineers (ASHRAE)[75]; the reading for all the nanofluids can be trusted. Fig. 2 shows the viscosity; specific heat capacity drops with the inclusion of nanofluids and continues to decline as the concentration and temperature increase. This is because of the nanoparticles' lower specific heat capacity values than water; where we look at the thermal conductivity, we see the opposite pattern.

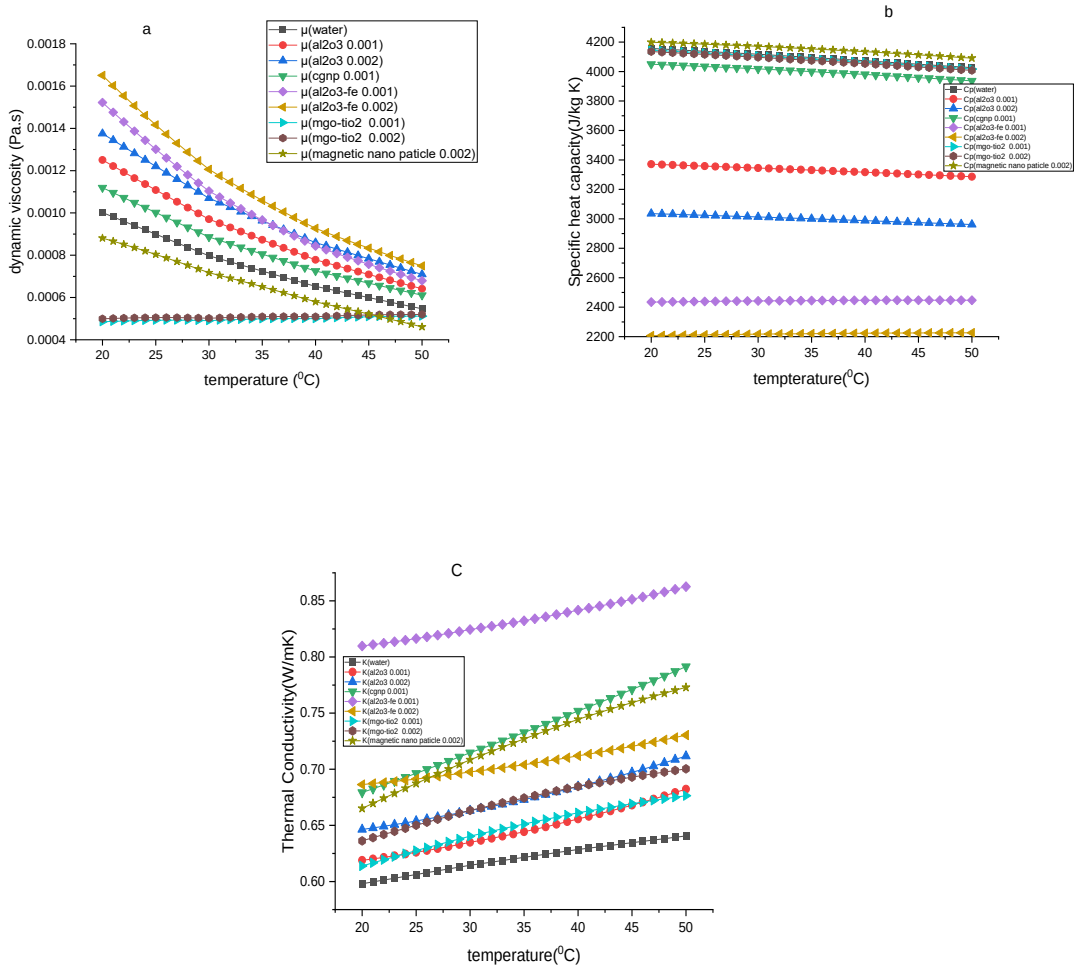

FIG 2 Thermophysical properties for (a) dynamic viscosity (b) specific heat capacity (c) thermal conductivity

5. THEORETICAL ANALYSIS

This section contains the mathematical equations used to model the flat plate collector . The system, nanofluid modelling, entropy formulation and fluid flow region are in detailed analysed in this sections. This study based on the premise that the system operates in a steady-state environment with a homogenous heat flux.

6.1 NANOFLUID MODELING AND VALIDATION

The thermophysical parameters of the nanofluids must be determined in order to calculate the heat transfer coefficient in the flow zone. It has been demonstrated that traditional formulas for estimating the thermo-physical properties of nanofluids can be used[76]. The results of the experiment are used to suggest a polynomial regressions model that predicts the viscosity, specific heat capacity, density and thermal conductivity of all nanofluids. The present models influenced by the temperature of fluid and nanoparticle volume %age. In this experiment, the basic fluid is water.

The thermal conductivity of nanofluid is :

$$k_{nf} = \left(a_0 + a_1 T_f + a_2 T_f^2 + a_3 \emptyset + a_4 \emptyset^2\right) k_{bf} \quad (1)$$

The specific heat capacity of nanofluid is :

$$C_{P_{nf}} = \left(a_0 + a_1 T_f + a_2 T_f^2 + a_3 \emptyset + a_4 \emptyset^2\right) C_{P_{bf}} \quad (2)$$

The viscosity of the nanofluid is :

$$\mu_{nf} = \left(a_0 + a_1 T_f + a_2 T_f^2 + a_3 \emptyset + a_4 \emptyset^2\right) \mu_{bf} \quad (3)$$

where Table 3 shows the constants of regression models stated in equations. The statistical coefficient of determination (R2) and root mean square values (RMS) are used to assess the reliability of the proposed models. The R2 values in Table are all greater than 0.95, demonstrating the models' excellent dependability in precisely predicting the attributes of specific heat capacity, density ,thermal conductivity, and viscosity.

TABLE 3. REGRESSION MODEL CONSTANTS

AUTHOR	LIMITATIONS	NANO FLUIDS	THERMAL PROPERTY	REGRESSION CONSTANTS a_0	a_1	a_2	a_3	a_4
Mousavi et al[50]	$10℃ \leq T \leq 70℃$ and $0.001 \leq \emptyset \leq 0.005$	Hybrid magnesium oxide-titanium oxide in water	K	0.944205	0.003011	-0.000029	31.87665	1819.797
			μ	0.290433	0.008206	0.000098	-21.4733	11926.04
			Cp	0.999944	-0.000025	0.0000006	-2.47987	58.32673
			ρ	1.001101	0.00000357	0	1.537174	108.6821
Shi et al[37]	$15℃ \leq T \leq 65℃$ and $0.002 \leq \emptyset \leq 0.006$	Magnetic nano particle(Ni, Fe3O4, Co3O4) in water	μ	0.65901	0.010016	-0.00016	35.29375	3382.672
			K	0.875434	0.00637	-0.000046	76.55851	-6341.06
			Cp	1.006208	0.000534	-0.0000048	-2.39885	-1.05805
Okonkwo et al[57]	$20℃ \leq T \leq 70℃$ and $0.0005 \leq \emptyset \leq 0.002$	Aluminium oxide in water	K	1.06333	-0.00311	0.0000588	-7.45244	17797.33
			Cp	0.85630	0.0000699	0.0000015	-30.6928	-16661.1
			μ	1.09721	-0.00462	0.0000303	285.1626	-53506.2
Sadri et al[34]	$15℃ \leq T \leq 50℃$ and $0.00025 \leq \emptyset \leq 0.001$	Clove treated graphene nanoplatelet(cgnp) in water	Cp	0.981968	0.000302	-0.000002	-8.48353	-4244.83
			μ	1.099703	-0.00222	0.0000317	-31.3761	81080.4
			K	0.941766	0.001219	0.00003	72.35941	85384.5
Okonkwo et al[57]	$20℃ \leq T \leq 70℃$ and $0.0005 \leq \emptyset \leq 0.002$	Hybrid Aluminium oxide-Fe in water	K	1.030067	-0.00375	0.00005	130.6383	-22138.6
			Cp	0.764603	0.000814	-0.000001	-264.762	69980.29
			μ	1.69324	-0.02428	0.000215	275.2056	-48992.7

The density of nanofluid (ρ_{nf}) is derived from the mixture rule. As such it can be represented as[77,78]:

$$\rho_{nf} = \frac{m_{bf}+m_{hnp}}{v_{bf}+v_{hnp}} = \frac{\rho_{bf}v_{bf}+\rho_{hnp}v_{hnp}}{v_{bf}+v_{hnp}} \quad (4)$$

The density of the nano fluid is given by:

$$\rho_{nf} = (1 - \emptyset_t)\rho_{bf} + \emptyset_t \rho_{hnp} \quad (5)$$

TABLE 4: DENSITY OF NANO FLUID AT DIFFERENT CONCENTRATIONS

Nanofluids at different concentrations	Density of nanofluids (Kg/m^3)
water	1000
Al_2O_3/ water at 0.1%	1002.9
Al_2O_3-Fe/ water at 0.1%	1010.7
CGNP/ water at 0.1%	1001.2
Al_2O_3-Fe/ water at 0.2%	1021.4
MgO-TiO_2/ water at 0.1%	1006.8
Al_2O_3/ water at 0.2%	1005.8
MgO-TiO_2/ water at 0.2%	1013.6
Magnetic nano particle(Ni)/ water at 0.2%	1006.9

where bf and hnp refer to the fluid and nanoparticle respectively and $\emptyset_t = \frac{v_{hnp}}{(v_{bf}+v_{hnp})}$ is the volume fraction of the nanoparticles .

the total volumetric concentration of the nanoparticles can be calculated as follows[79]:

$$ø = \%\ \text{volumetric concentration} = \frac{\frac{w_{np}}{\rho_{np}}}{[\frac{w_{np}}{\rho_{np}}]+v_b} \times 100 \quad (6)$$

$$\emptyset_t = \sum_{i=1}^{nnp} \emptyset_i \quad (7)$$

$$\rho_{hnp} = \frac{\sum_{i=1}^{nnp} \emptyset_i \rho_i}{\sum_{i=1}^{nnp} \emptyset_i} \quad (8)$$

where w_{np} is the weight of the nanoparticle, ρ_{np} nanoparticle density, v_b accounts for the volume of the base fluid and nnp represents nanoparticles number respectively.

The heat transfer coefficient (h_{nf}) is a parameter in the nanofluid flow within the flat plate collector. Heat transfer coefficient depends on Nusselt number and calculated as follows[80]:

$$h_{nf} = \frac{Nu\,.\,k_{nf}}{D_i} \quad (9)$$

The Reynolds and Prandtl numbers are calculated as follows[81]:

$$Re = \frac{4m}{\pi D_i \mu_{nf}} \quad (10)$$

$$Pr = \frac{\mu_{nf} cp_{act_{nf}}}{k_{nf}} \quad (11)$$

The Nusselt number of nanofluids calculated by applying Pak and Cho corelation is[82]:

$$Nu = 0.021 \times Re^{0.8} \times Pr^{0.5} \quad (12)$$

After expanding above equation

$$h_{nf} = 4.2610 \times {k_{nf}}^{0.5} \times \frac{Cp_{nf}^{0.5}}{\mu_{nf}^{0.3}} \quad (13)$$

Equation for evaluation of friction factor for nanofluid flow[83]:

$$f = 0.3108 \times Re^{-0.245} \times (1 + \emptyset)^{0.42} \quad (15)$$

Since $2000 < Re < 22000\,; 0 < \emptyset < 0.006$

The Nusselt number for water calculated according to Gnielinski's equation[24] :

Since $2000 < Re < 10^5\,; 0.6 < Pr < 2000$

So regarding equation is

$$\frac{h\times D_i}{k} = \frac{(0.125f)\times(Re-1000)\times Pr}{1+12.7\times(0.125f)^{0.5}\times(Pr^{0.667}-1)} \quad (16)$$

$$friction\ factor(f) = (1.58lnRe - 3.82)^{-2} \quad (17)$$

6.2 ENERGY AND EXERGY ANALYSIS

Energy is conserved, according to the fundamental law of thermodynamics, and the total amount of conserved energy remains constant. Different sorts of energies (such potential, kinetic, and internal) can, nevertheless, be converted from one form to another. The law can be used to express an energy balance[84].

$$\frac{dE}{dt} = \sum\frac{dQ}{dt} - \sum\frac{dW}{dt} + \sum\frac{dm_i}{dt}(h_i + \frac{v_i^2}{2} + gz_i) - \sum\frac{dm_0}{dt}\left(h_0 + \frac{v_0^2}{2} + gz_0\right) \quad (18)$$

The differential form of the specific equation is:

$$de = \delta q - \delta w - dh - dke - dPe \quad (19)$$

The absorbing medium potential heat gain (Q_u) is defined as

$$Q_u = \frac{dm}{dt}Cp_{nf}\left(T_{f,out} - T_{f,in}\right) \quad (20)$$

It is also measured by means of the amount of heat carried away in the nano fluid passed through collector ;If I is the solar radiation intensity, expressed in W/m2, as solar radiation falls on solar collector's plate. If the collector's surface area is A, m2, the solar radiation it receives is[85]:

$$Q_i = IA \qquad (21)$$

However, some of the radiation is reflected back to the sky, while another portion is absorbed by the glass cover and the remainder is transmitted through it, reaching the absorber plane as short-wavelength radiation. As a result, the conversion factor is difference between proportion of solar energy that passes through collector's transparent cover (transmission) and the %age that is absorbed. It is essentially the product of the rate of transmission through the glass cover and the rate of absorption of the absorber plane.

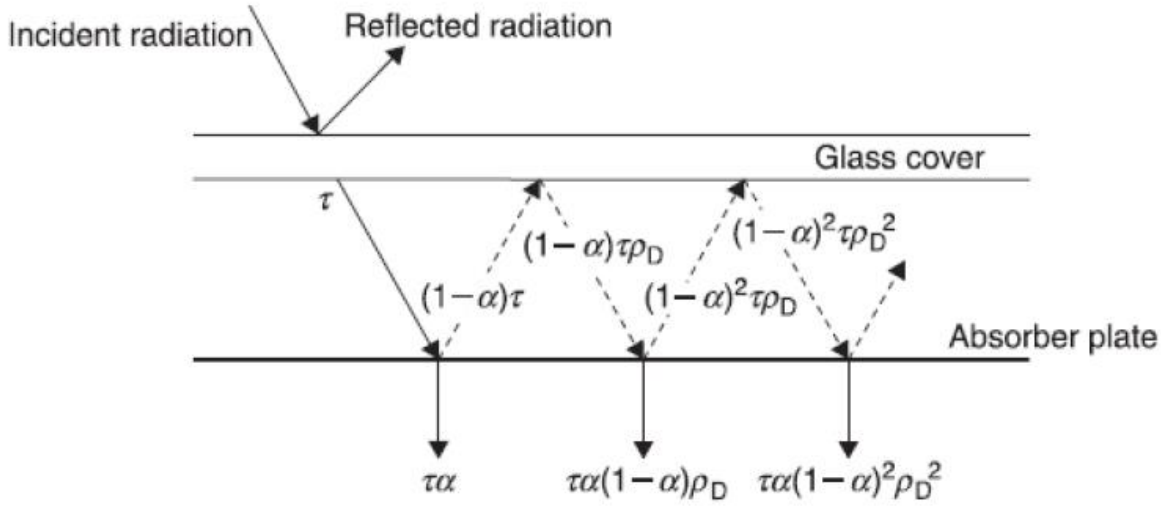

FIG 3: sun radiation absorption by an absorber plate underneath a cover system

The incident energy falling on the collector plate , τα is absorbed by the absorber plate and (1 - α) τ is reflected back by the glass cover. The reflection from the absorber plate is called diffuse, so (1 - α) τ penetrates glass cover is the diffuse radiation and $(1-\alpha)\tau\rho_D$ is reflected back to absorber plate. Multiple reflections of dispersed radiation take place, allowing some of the sun energy to be absorbed.

AVERAGE TRANSMITTANCE-ABSORPTANCE PRODUCT CALCULATION

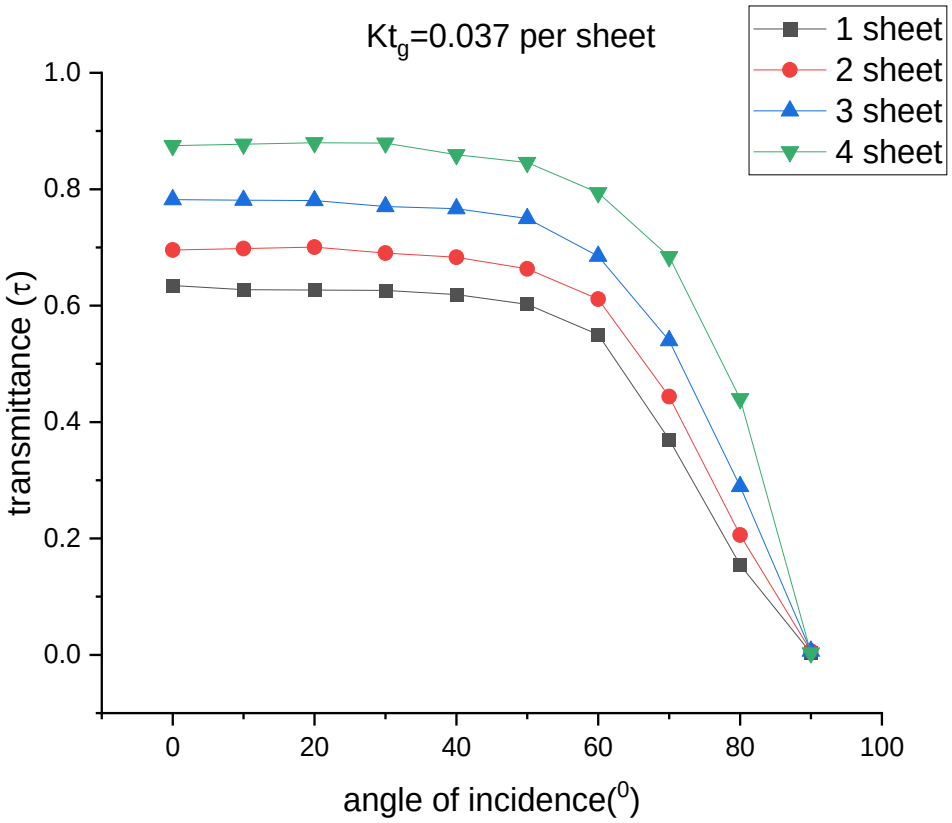

FIG 4 Transmittance of glass's 1, 2, 3, and 4 coverings, taking absorption and reflection into account.

In general explanation it applicable for beam, diffuse, and ground radiation also[86]

$$\text{n} = \text{refractive index of light} = \frac{\text{c}}{\text{v}}$$

C= speed of light , v= speed of light in that medium

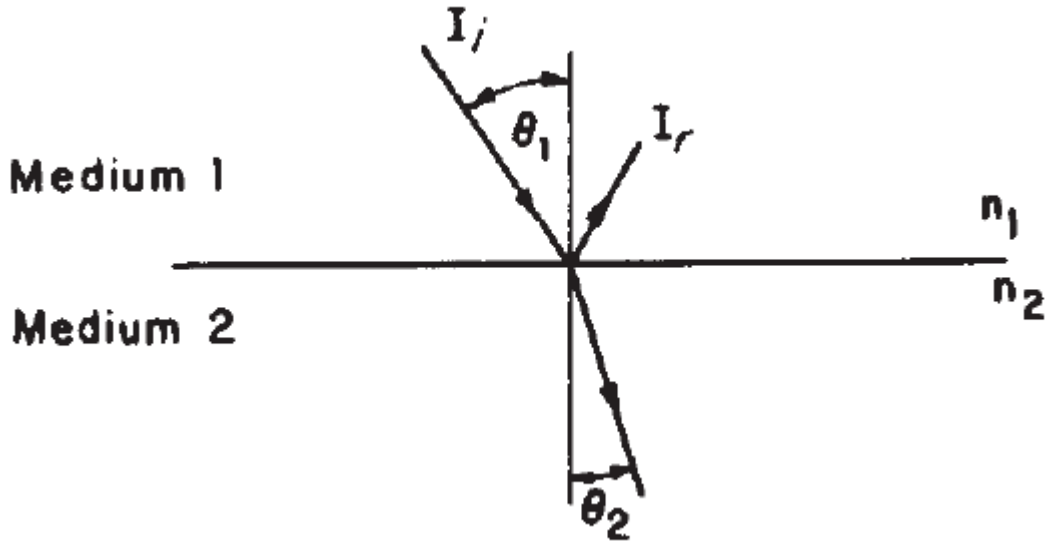

FIG 5. Angles of refraction and incidence in materials with n1 and n2 refractive indices.

$$n_1 \sin\theta_1 = n_2 \sin\theta_2$$

$$\theta_1 = \text{incident angle}$$

$$\theta_2 = \text{refraction angle}$$

$$n_1, n_2 = \text{refractive indices of medium 1 , medium2}$$

$$\tau_a = \text{transmittance of absorber plate} = \frac{I_{transmitted}}{I_{incident}}$$

$$= \exp\left(-\frac{Kt_g}{\cos\theta_2}\right)$$

K= extinction coefficient

t_g= thickness of glass cover

Reflectance of diffused radiation

$$\rho_D = \tau_a - \tau \quad (22)$$

average transmittance-absorptance product is

$$(\tau\alpha)_{avg} = \frac{\tau\alpha}{1-(1-\alpha)\rho_D} \quad (23)$$

Thus[85],

$$Q_i = I(\tau\alpha)_{avg}A \quad (24)$$

After absorbing heat, the temperature of the collector rises above the ambient temperature, and heat is released through convection and radiation. The overall heat transfer coefficient of the collector (U_L) and the temperature of the collector determine the rate of heat loss (Q_0)[88].

$$Q_0 = U_L A(T_P - T_0) \quad (25)$$

As a result, the collector's rate of useful energy driven (Q_U) is proportional to the collector's rate of useful energy absorbed and the quantity of useful energy lost to the environment.

This is expressed as[87]:

$$Q_U = Q_i - Q_o = I(\tau\alpha)_{avg} A - U_L A(T_P - T_0) \quad (26)$$

Thermal efficiency (η) of a flat plate collector is defined as the ratio of useful energy (Q_U) to the total incident solar radiation on the collector surface.

$$\eta = \frac{Q_U}{IA} \quad (27)$$

The summation of heat loss of the collector from the top (U_t), from the sides (U_S), and at the bottom of the collector (U_{bc}) is the overall loss in the system[87].

$$U_L = U_t + U_{bc} + U_s \quad (28)$$

The top loss coefficient (U_t) is calculated by

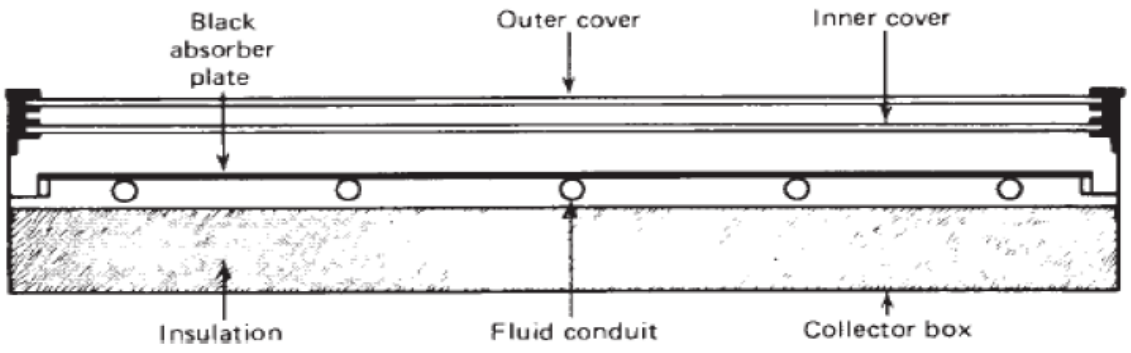

FIG 6. basic flat plate solar collector's cross section

The following are the assumptions:

1. a state of equilibrium

2. The structure is made up of parallel tubes.

3. A little collector area near headers can be overlooked.

4. a consistent flow into the tubes

5. No solar energy absorption by the cover

6. Temperature drop via a cover is minor.

7. Infrared radiation is blocked by the coverings.

8. For long-wavelength radiation, the sky can be considered a blackbody.

9. Temperature gradients in the vicinity of tubes can be ignored.

10. Temperature differences in the flow direction and between the tubes can be neglected.

$$U_t = \left(\frac{1}{h_w} + \frac{N}{\frac{C}{T_{pm}}\left[\frac{T_{pm}-T_0}{N+f}\right]^e}\right)^{-1} + \frac{\sigma(T_{pm}+T_0)(T_{pm}^2+T_0^2)}{\frac{1}{\epsilon_p+0.00591Nh_w}+\frac{2N+f-1+0.133\epsilon_p}{\epsilon_g}-N} \quad (29)$$

$$h_w = \frac{8.6v_w^{0.6}}{L^{0.4}} \quad (30)$$

$$f = \left(1 + 0.089h_w - 0.1166h_w\epsilon_p\right)(1 + 0.07866N) \quad (31)$$

$$C = 520(1 - 0.000051\beta^2)\ for\ 0° < \beta < 70° \quad (32)$$

$$e = 0.430\left(1 - \frac{100}{T_{pm}}\right) \quad (33)$$

Where, N = number of glass cover

β = collector tilt (deg) angle

ε_g= emittance of glass (0.88)

ε_p= emittance of plate

T_0= ambient temperature (K)

T_{pm}= mean plate temperature (K)

h_w= wind heat transfer coefficient (W/m^2 ◦C)

The FPC's bottom heat loss is influenced by the thermal conductivity and insulator thickness. As shown below, the bottom heat loss is computed. [89]

$$U_{bc} = \frac{1}{\frac{t_b}{k_b}+\frac{1}{h_b}} \quad (34)$$

heat loss co efficient from the sides of the solar collector is given by

$$U_s = \frac{1}{\frac{t_s}{k_s}+\frac{1}{h_s}}\frac{A_s}{A} \quad (35)$$

where t_b, t_s, k_b, k_s, and A_s, respectively, stand for the bottom insulation thickness, side insulation thickness, bottom insulation thermal conductivity, side insulation thermal conductivity, and side insulation surface area.

U_t is reliable on absorber plate temperature T_p and similarly, U_L is on T_p.

The usable energy gain of a collector is the complete surface of the collection was at inlet temperature of fluid. "Collector heat removal factor (F_R)" is the term for this.

and is expressed as[85]:

$$F_R = \frac{mCp_{nf}(T_P - T_0)}{A[I\tau\alpha - U_L(T_P - T_0)]} \quad (36)$$

When the entire solar collector is at the incoming fluid temperature, the maximum usable energy gain occurs. Multiplying the collector heat removal factor (F_R) and the maximum usable energy gain yields the actual useful energy gain (Q_U).

$$Q_u = F_R A[I\tau\alpha - U_L(T_P - T_0)] \quad (37)$$

widely used relationship to measure collector energy gain is known as the “Hottel-Whillier-Bliss equation”.

The collector efficiency (η) of flat plate collector is defined by the ratio of the useful energy gain (Q_U) to the total solar energy incident on collector surface during a certain time:

$$\eta = \frac{\int Q_u dt}{A \int I dt} \quad (39)$$

The instantaneous thermal efficiency is

$$\eta = \frac{Q_u}{A.I} \quad (40)$$

$$\eta = F_R \tau\alpha - F_R U_L \left(\frac{T_P - T_0}{I}\right) \quad (41)$$

Equation obtain for plate temp[90]:

$$T_P = T_{in} + \frac{Q_U(1-F_R)}{AU_L F_R} \quad (42)$$

The collector heat removal factor is used to express the overall usable energy gain of a solar collector due to the inlet temperature of nanofluid. When collector surface is at local nano fluid temperature, heat removal factor is given as the ratio of actual usable gain in energy. Symbolically expressed as[90]:

$$F_R = \frac{mCp_{nf}}{AU_L}\left[1 - exp\left(-\frac{U_L F\prime A}{mCp_{nf}}\right)\right] \quad (44)$$

Here F' is collector efficiency factor, given below[90]:

$$F' = \frac{\frac{1}{U_L}}{W\{\frac{1}{U_L[D+(W-D)F]} + \frac{1}{C_b} + \frac{1}{\pi D_i h_{nf,i}}\}} \quad (45)$$

where W= tube spacing in collector

D= risers outer diameter

h_{nfi}= the heat transfer coefficient

D_i= risers inner diameter

C_b is bond conductance, bond coductivity k_b , γ accounts for the average bond thickness, and the b is the bond width,. The bond conductance per unit length is :

$$C_b = \frac{k_b b}{\gamma} \qquad (46)$$

The factor F is standard fin efficiency is given by:

$$F = \frac{\tanh[\frac{m(W-D)}{2}]}{\frac{m(W-D)}{2}} \qquad (47)$$

$$m = \sqrt{\frac{U_L}{k\delta}} \qquad (48)$$

5.3 ENTROPY GENERATION FORMULATION

Exergic efficiency is defined as the maximum useable work that the system produce and it is determined as given by[91]::

$$\eta_{ex} = \frac{E_U}{E_{sun}} \qquad (49)$$

where E_u andE_{sun} accounts for the exergic output of the solar plate collector and sun respectively. Solar exergy is calculated by equation[92]

$$E_{sun} = AI_t \left[1 - \frac{4}{3}(\frac{T_0}{T_{sun}}) + \frac{1}{3}(\frac{T_0}{T_{sun}})^4\right] \qquad (50)$$

The exergetic output is computed using equation to account for the irreversibilities due to the heat transfer and pressure losses in the system[93].:

$$E_u = Q_u - mCp_{bf}T_0\left[\left\{(a_0 + a_3\emptyset + a_4\emptyset^2)ln\left(\frac{T_{out}}{T_{in}}\right)\right\} + \left\{(T_{out} - T_{in})\left(a_1 + \frac{a_2}{2}(T_{out} + T_{in})\right)\right\}\right] - mT_0\frac{\Delta P}{\rho_{nf}T_P} \qquad (51)$$

where ΔP is given by pressure drop, pumping power is given by[94]:

pumping power loss $= \frac{\mathrm{m}}{\rho_{\mathrm{nf}}} \times \Delta \mathrm{P}$.

Exergy analysis of solar collectors aids designers in determining the best design and reducing exergy losses. The Exergy notion is one method, and entropy generation from irreversibility's is the other method for analysing the second law. Both methods get the same outcomes. Exergy efficiency and the shares of irreversible variables can both be calculated using exergy balance on a solar collector. Exergy balance on a solar collector with a flat plate

$$\sum \frac{dE_{in}}{dt} - \sum \frac{dE_{out}}{dt} - \sum \frac{dE_{loss}}{dt} - \sum \frac{dE_{change}}{dt} - \sum \frac{dE_{des}}{dt} = 0 \quad (52)$$

Exergy intake rate E_{in} comprises exergy associated with mass flow rate and solar radiation exergy, whereas exergy output rate includes exergy mass flow. The exergy accumulated by the nano fluid flow is called E_{gain}.

$$\frac{dE_{gain}}{dt} = \frac{dE_{out,f}}{dt} - \frac{dE_{in,f}}{dt} \quad (53)$$

where E_{in} is exergic rate at inlet, E_s is stored exergy rate, E_{out} is exergic rate at outlet, and E_{loss} is exergy loss rate.

At steady condition $E_s = 0$

The loss of work (W_{lost}) to environment is necessary to calculate the entropy generation rate of the collector. This connection is given by[95]

$$S_{gen} = \frac{E_d + E_{loss}}{T_0} = \frac{W_{lost}}{T_0} \quad (54)$$

The surroundings exergic loss is obtained by

$$E_{loss} = U_L A (T_P - T_0)(1 - \frac{T_0}{T_P}) \quad (55)$$

The exergy destroyed (E_d) in the collector due to irreversibilities within the system is defined as [96]

$$E_d = E_{d,\Delta p} + E_{d,\Delta Ts} + E_{d,\Delta Tf} \qquad (56)$$

The exergy lost as a result of pressure losses in the system brought on by the heat transfer fluid's friction is given as:

$$E_{d\Delta P} = T_0 m \frac{\Delta P}{\rho_{nf}} \frac{\ln(\frac{T_{out}}{T_0})}{(T_{out}-T_{in})} \qquad (57)$$

The energy loss brought on by the absorber plate's temperature difference from the sun When stated as $E_{d,\Delta Ts}$ is expressed as :

$$E_{d,\Delta Ts} = (\tau\alpha)_{eff} I_t A T_0 \left(\frac{1}{T_P} - \frac{1}{T_{sun}}\right) \qquad (58)$$

An expression ($E_{d,\Delta Tf}$) is provided for calculating the exergy lost as a result of the working fluid flowing through the collector tubes is given as:

$$E_{d,\Delta Tf} = mCp_{bf} T_0 \left[\left[\left\{(a_0 + a_3\emptyset + a_4\emptyset^2) ln\left(\frac{T_{out}}{T_{in}}\right)\right\} + \left\{(T_{out} - T_{in})\left(a_1 + \frac{a_2}{2}(T_{out} + T_{in})\right)\right\}\right] - \left[\left(\frac{1}{T_P}\right)\left\{(a_0 + a_3\emptyset + a_4\emptyset^2)\left(\frac{T_{out}^2 - T_{in}^2}{2}\right) + \frac{a_1}{3}(T_{out}^3 - T_{in}^3) + \frac{a_2}{4}(T_{out}^4 - T_{in}^4)\right\}\right]\right] \qquad (59)$$

The first part of Equation accounts for overall exergy losses in the system, which include thermal losses in the collector due to the thermodynamic reasons and optical losses occurs because of optical flaws in the solar plate collectors.
The system's exergy destruction is accounted for in the second part.
This exergic destruction is sum of thedestruction caused by heat transfer from the sun to the r eceiver and the exergy destruction caused by heat transfer from the absorber plate of solar collector to the working nanofluid.

The end statement denotes loss of exergy owing to frictional flow in the working fluid .

Overall entropy generated in the system is owing to irreversibility of the temperature gradient due to the heat transfer of nanofluids ($S_{gen}(H)$) and pressure of nanofluids in tube ($S_{gen}(P)$).

The total entropy generation in the system comes due to the irreversibility of heat transfer due to temperature gradients ($S_{gen}(H)$) and pressure losses due to fluid friction ($S_{gen}(F)$). Equation shows this relationship, which is used here to calculate the entropy generation rate in the solar plate collector.

$$S_{gen} = \frac{E_{loss}+E_d}{T_0} = \frac{U_L A(T_P-T_0)\left(1-\frac{T_0}{T_P}\right)+(\tau\alpha)_{eff} I_t T_0 A\left(\frac{1}{T_P}-\frac{1}{T_{sun}}\right)+ mCp_{bf}T_0\left[\left[\left\{(a_0+a_3\emptyset+a_4\emptyset^2)ln\left(\frac{T_{out}}{T_{in}}\right)\right\}+\left\{(T_{out}-T_{in})\left(a_1+\frac{a_2}{2}(T_{out}+T_{in})\right)\right\}\right]-\left[\left(\frac{1}{T_P}\right)\left\{(a_0+a_3\emptyset+a_4\emptyset^2)\left(\frac{T_{out}^2-T_{in}^2}{2}\right)+\frac{a_1}{3}(T_{out}^3-T_{in}^3)+\frac{a_2}{4}(T_{out}^4-T_{in}^4)\right\}\right]\right]+mT_0\frac{\Delta P}{\rho_{nf}(T_{out}-T_{in})}\frac{\ln(\frac{T_{out}}{T_{in}})}{T_0}} \quad (60)$$

The Bejan number is the ratio of the system's overall entropy generation (S_{gen}) to the irreversibilities from heat transfer ($S_{gen(H)}$) and is calculated by equation[97]

$$Be = \frac{S_{gen(H)}}{S_{gen}} \quad (61)$$

6. RESULT AND DISCUSSION

In this part, the performance of 5 different types of nanofluids are evaluated. This assessment made using the parameters such as inlet temperature of nanofluids, mass flow rate in tubes of collector, and volumetric fraction of nanoparticle.

6.1 HEAT TRANSFER COEFFICIENT

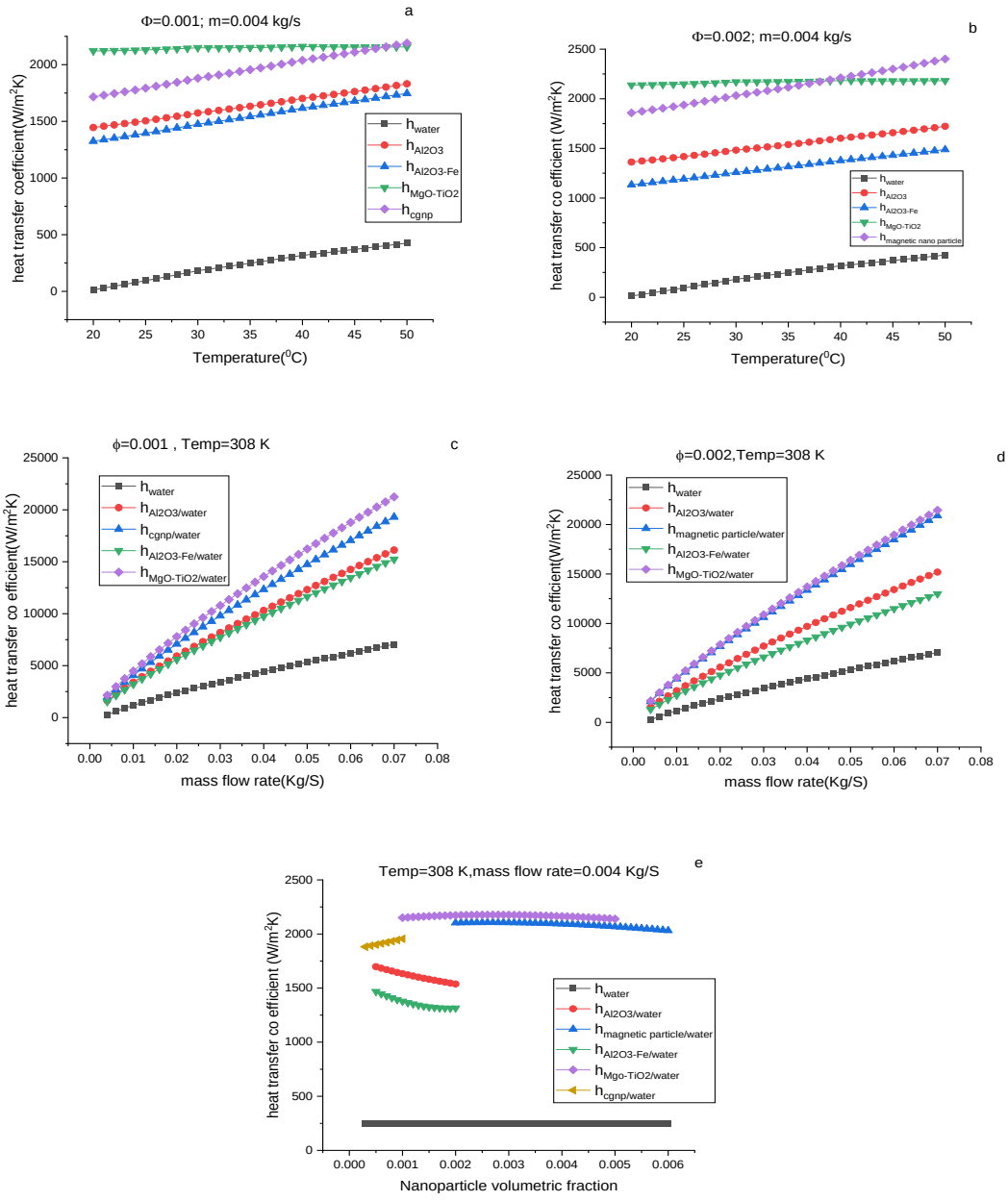

FIG. 7. Heat transfer coefficient as a function of (a,b) temperature (c,d) mass flow rate (e) nano particle volumetric fraction

The performance of the solar collector is significantly influenced by the heat convection coefficient. This parameter is influenced by the working fluid's mass flow rate, flow zone geometry, and temperature characteristics. Fig. 7 illustrates how the mass flow rate and temperature increase in the flat plate collector benefits in the heat convection coefficient. According to Fig. 7(a) , 7(,b), utilising Al_2O_3-Fe/water , clove treated graphene nanoplatelet/water , MgO-TiO_2/water , magnetic particle/water and Al_2O_3/water nanofluids, respectively, results in a mean improvement in heat transfer coefficient at constant mass flow rate 85, 88 , 89 , 89 ,85 %.Here from calculation it is found that with the increase in temperature the MgO-TiO_2/water , magnetic particle/water have highest heat transfer co efficient .With the increasing mass flow rate the mean % improvement in heat transfer coefficient for Al_2O_3-Fe/water, clove treated graphene nanoplatelet/water, MgO-TiO_2/water, magnetic particle/water, and Al_2O_3/water nanofluids, respectively, is 55, 65, 68, 67, and 58 % at constant temperature and volumetric fraction. Here from calculation it found that MgO-TiO_2/water has highest heat transfer coefficient with increasing mass flow rate as shown in Fig. 7(c) , 7(d). This improvement is observed to grow with temperature, mass flow rate indicating that higher temperatures, mass flow rate more useable energy is produced due to increase in heat loss coefficient , which improves performance . A decrease in heat transfer coefficient observed in MgO-TiO_2/water , Al_2O_3-Fe/water , magnetic particle/water and Al_2O_3/water nanofluids and also increment is found in clove treated graphene nanoplatelet/water with the increase in volumetric fraction as shown in Fig. 7(e). From Fig. 7€ it is found that at a 0.26% volumetric fraction MgO-TiO_2/water, magnetic particle/water have maximum heat transfer coefficient similarly at 0.05% volumetric fraction Al_2O_3-Fe/water, Al_2O_3/water have highest heat transfer coefficient and at 0.1% clove treated graphene nanoplatelet/water shows highest heat transfer.

6.2 NUSSELT NUMBER

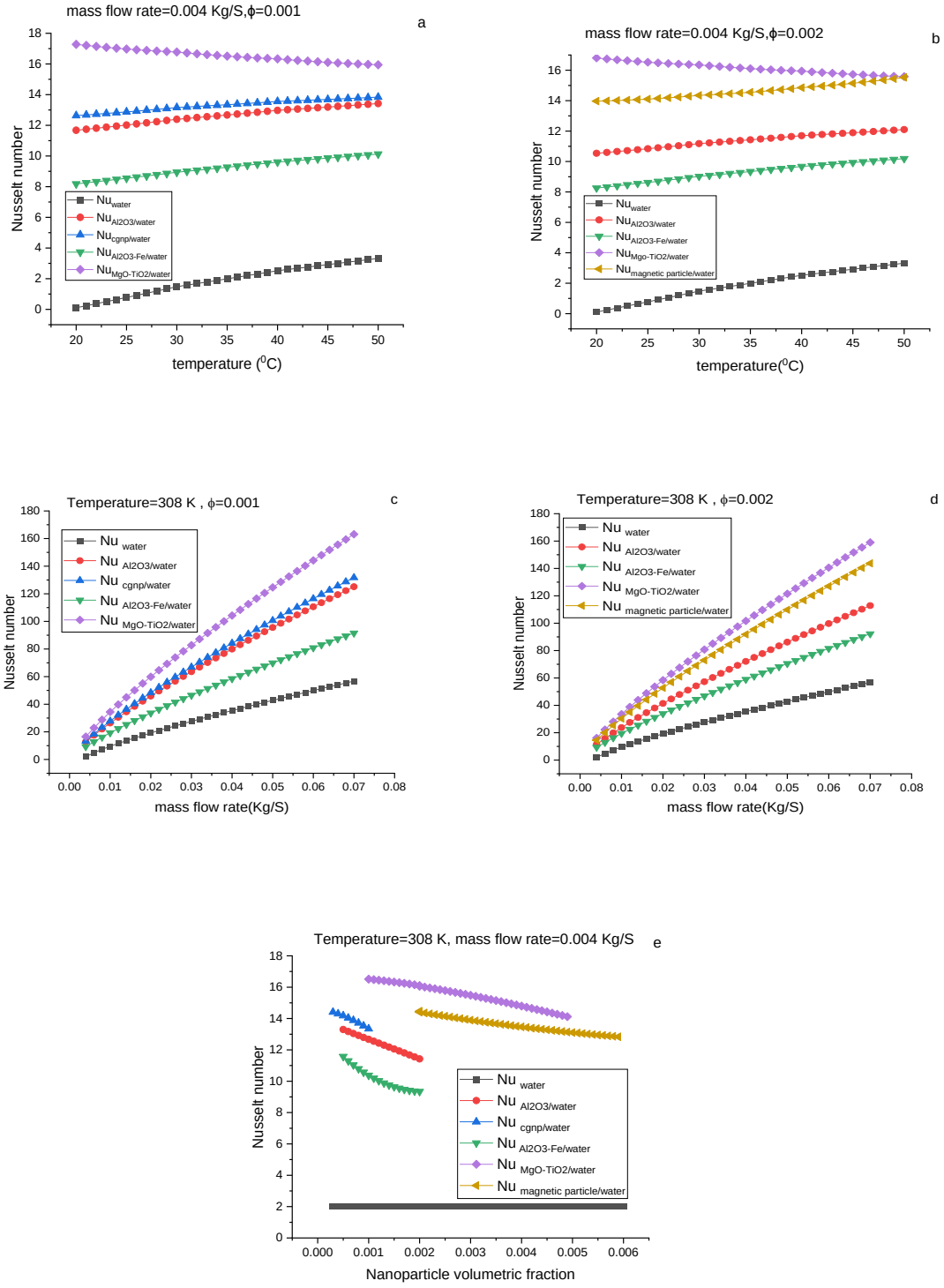

FIG. 8. Nusselt number as a function of (a,b) temperature (c,d) mass flow rate (e) nano particle volumetric fraction

Brownian diffusion and thermophoresis determine the Nusselt number of nanofluid inside the tube. The Nusselt numbers, which illustrate how nanoparticles improve heat transfer coefficient with mass flow rate and temperature, are shown in the Fig. 8. In general, increasing the Reynolds number will raise the Nusselt number in fluids, and the same is true for nanofluids. However, for a given Re number and a given nanoparticle, increasing the nanofluid concentration causes the Nu to decrease. However, as the temperature is raised for a given concentration, this trend is reversed, and rising temperatures cause the Nusselt number to fall because of sharply increased thermal conductivity as here the case of MgO-TiO_2/watere. For various materials, this particular outcome is different. According to Fig. 8(a), 8(,b), for a given temperature range, constant volumetric fraction, and nanofluid mass flow rate, the mean %age increment in the Nusselt number is highest for MgO-TiO_2/water, which is 88 %, followed by 87,86,85,79 % for magnetic particle/water, clove-treated graphene nanoplatelet/water, Al_2O_3/water, and Al_2O_3-Fe/water, respectively. With different mass flow rates and constant temperature, a similar pattern of Nusselt number was obtained, as shown in Fig. 8(c) 8(,d), where the mean % of Nusselt number is higher for MgO-TiO_2/water, followed by magnetic particle/water, clove-treated graphene nanoplatelet/water, Al_2O_3/water, and Al_2O_3-Fe/water, with respective values of 65,61,58,56, and 39 %. As can be observed in the Fig. 8(e), the Nusselt number of nanofluids in water base fluid decreases as the volumetric % of nanoparticles increases. All the nanofluids have high Nusselt number initially such as at 0.1%,,0.2% , 0.05%,0.03%,0.2% magnetic particle/water, clove-treated graphene nanoplatelet/water, Al_2O_3/water, and Al_2O_3-Fe/water, MgO-TiO_2/water have hight heat transfer rate.

6.3 REYNOLDS NUMBER

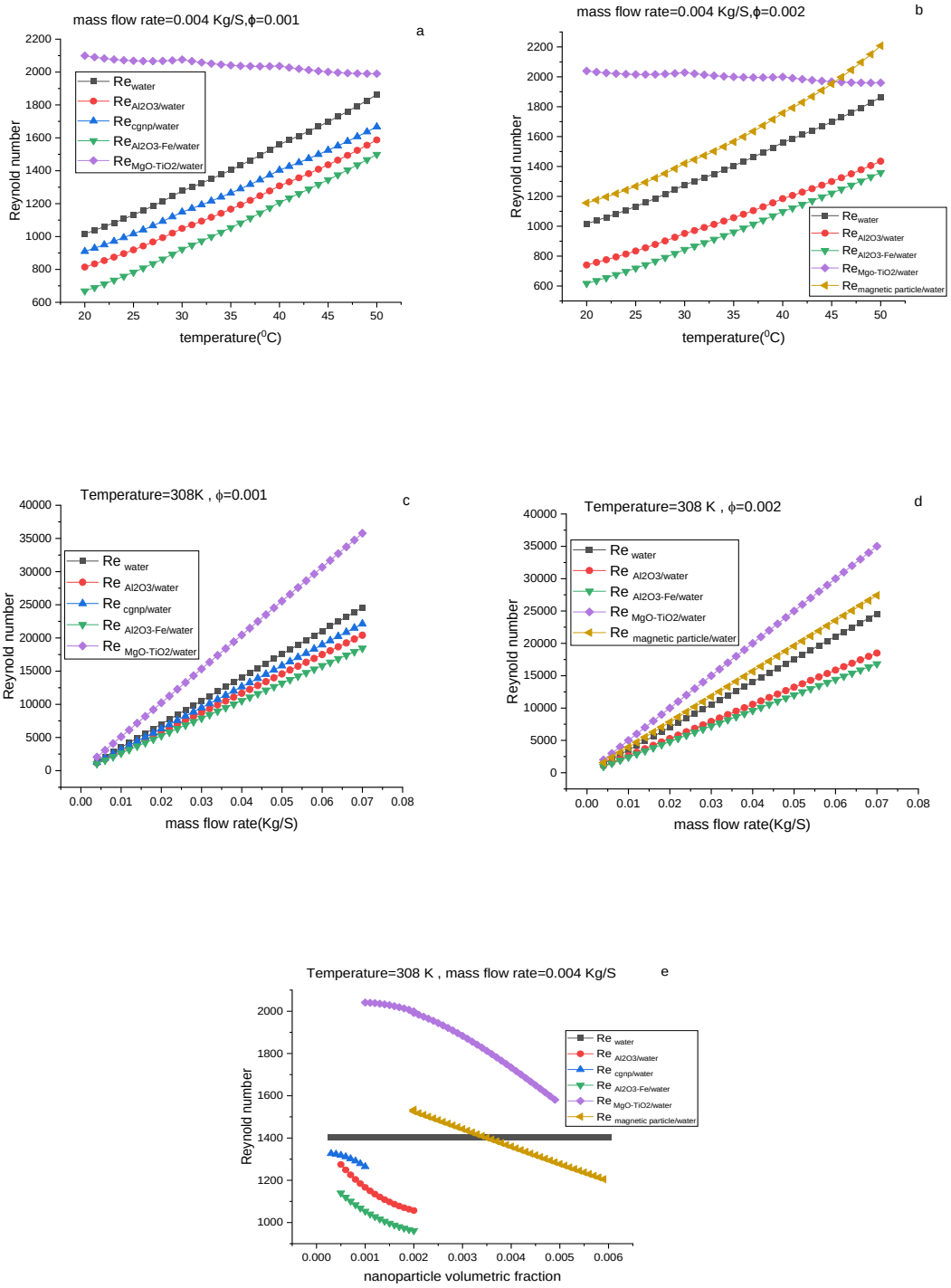

FIG. 9. Reynold number as a function of (a,b) temperature (c,d) mass flow rate (e) nano particle volumetric fraction

Fig. 9 looks at the mass flow rate, temperature, volumetric fraction, of Reynolds number of each nanofluid. Due to the varying viscosities of each fluid, the Reynolds numbers for each nanofluid vary for the similar mass flow rate, temperature, volumetric fraction. Fig. 9 shows that as temperature , mass flow rate rise, Reynolds number rises for all fluids. This is significant because as Reynolds number rises, heat resistance between the working fluids and the tube walls decreases. The convection thermal resistance would dramatically decrease at the higher Reynolds numbers when it is compared with the overall thermal resistance across the flat plate collector, despite the fact that nanofluids thermal conductivity value is higher. In general, when the temperature rises, the Reynolds number will rise in nanofluids due to a drop in the absolute viscosity value. However, in some nanofluids, opposite tendencies have also been seen because as the temperature rises, the pressure drop in the pipe reduces. The temperature also affects the pressure drop in the pipe, and as the temperature of the incoming fluid rises, the viscosity of the fluid also rises, raising Newton's viscosity fiction force. As a result, as the flow temperature rises, the Reynolds number in the pipe lowers. The mean % increase in Reynolds number with rise in temperature for MgO-TiO_2/water and magnetic particle/water is higher than water by 30,12%, but this value is lower for Al_2O_3/water, clove-treated nanoplatelet/water, and Al_2O_3-Fe/water. The mean % increase in Reynolds number with rise in mass flow rate is higher for MgO-TiO_2/water and magnetic particle/water is higher by 31.30%,10.3% respectively , follows by other nanofluids.In Fig. 9(e) it is shown that with the increase of volumetric concentration Reynolds number for all the nanofluids decreases and it is maximum for MgO-TiO_2/water at 0.1% volumetric fraction.

6.4 PRANDTL NUMBER

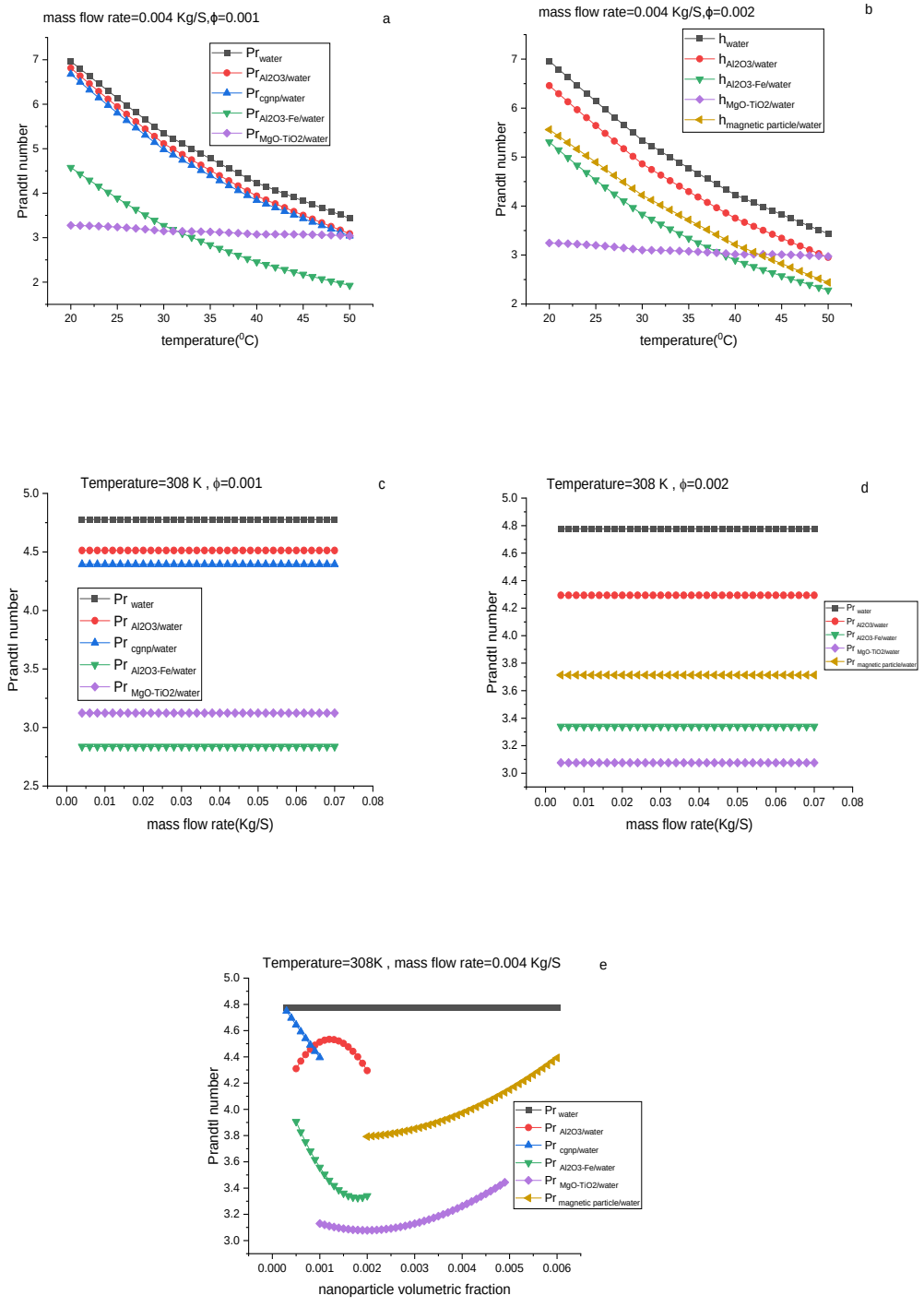

FIG. 10. Prandtl number as a function of (a,b) temperature (c,d) mass flow rate (e) nano particle volumetric fraction

The relationship between a nanofluid's viscosity and thermal conductivity is established by the Prandtl number, a dimensionless quantity. As a result, it evaluates the relationship between momentum transport and a fluid's capacity for thermal transport. The increase in thermal conductivity balances out the rise in viscosity, which makes the decrease in specific heat predominate. This is how the Prandtl number decrease can be explained. According to the Fig 10, Prandtl number falls as temperature rises while staying constant when mass flow rate increases. Because viscosity and heat conductivity are balanced in MgO-TiO_2/water, the prandtl number stays constant. viscosity values for magnetic particle/water and MgO-TiO_2/water are higher and for clove-treated graphene nanoplatelet/water, Al_2O_3-Fe/water thermal conductivity plays a significant role, mixed trends in prandtl numbers are obtained with an increase in nanoparticle volumetric fraction at fixed temperature. Al_2O_3-Fe/water has the lowest prandtl number in this case with a constant mass flow rate, followed by MgO-TiO_2/water, magnetic particles/water, clove-treated graphene nanoplatelets/water, and Al_2O_3/water, with respective values of 65,57,29,8,5 %. The minimum graph is produced for Al_2O_3-Fe/water at 0.1 % volumetric fraction and MgO-TiO_2/water at 0.2 % volumetric fraction since the prandtl number is independent of mass flow rate. The Al_2O_3-Fe/water, MgO-TiO_2/water, and Prandtl number of 68,55 % at 0.1 and 0.2 % volumetric fraction, respectively.The Prandtl number is maximum initially for clove-treated graphene nanoplatelets/water, and Al_2O_3-Fe/water at 0.03% and 0.05% but it is maximum at 0.5% ,0.6% for MgO-TiO_2/water, magnetic particles/water, si,ilarly it maximum 0.11% for Al_2O_3/water where it initially increases then decreases.

6.5 FRICTION FACTOR

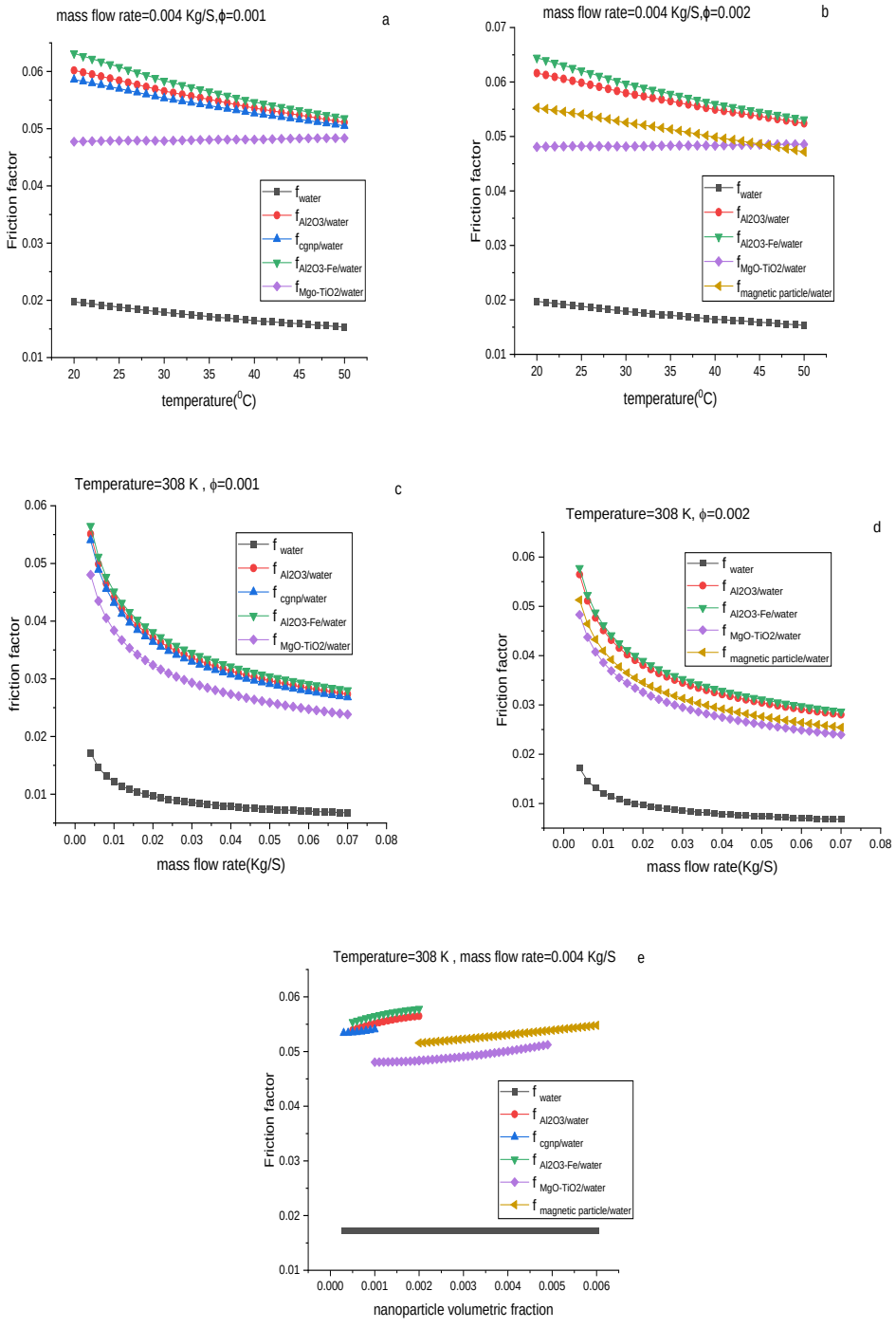

FIG. 11. Friction factor as a function of (a,b) temperature (c,d) mass flow rate (e) nano particle volumetric fraction

The pressure drop within the system is calculated using the friction factor, a dimensionless parameter that gives measurement of the shear stress that the flow places on a pipe's wall. Fig. 11 (a), 11(,b) shows that this parameter reduces as temperature rises because the working fluid has a lower viscosity at higher temperatures. The behaviour of the friction factor for the nanofluids under consideration is similar to the behaviour of the fluids' viscosity, demonstrating the close relationship between the two parameters. Fig. 11(c),11(,d) illustrates this relationship by showing how the working fluids' friction factor decreases as the mass flow rate rises and a rise in friction factor shown in Fig. 11 (e) with the increase of nano particle volumetric fraction. This is due to the fact that adding nanoparticles to water makes the nanofluid more viscous dynamically, which raises the friction factor. Al_2O_3-Fe/water has the highest friction factor at a constant mass flow rate as temperature rises, followed by Al_2O_3/water, clove-treated graphene nanoplatelets/water, magnetic particles/water, and MgO-TiO_2/water. When we evaluate it at constant temperature with increasing mass flow rate, we get a similar outcome.An increasing trend in nanoparticle volumetric fraction is shown in Fig. 11 (e) with constant temperature and mass flow rate and the value of friction factor is highest for Al_2O_3-Fe/water .

6.6 ABSORBED ENERGY PARAMETER

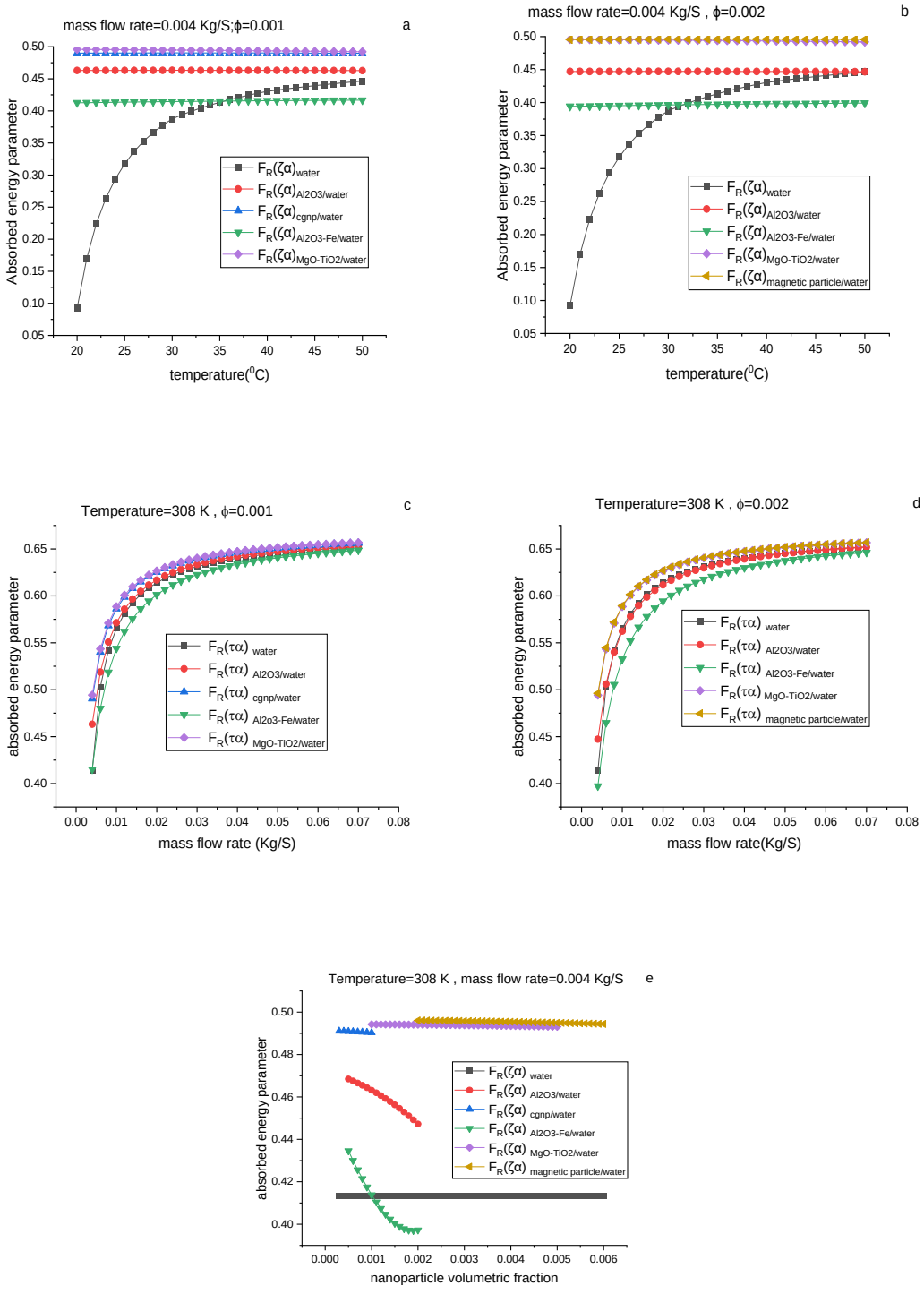

FIG. 12. Absorbed energy parameter as a function of (a,b) temperature (c,d) mass flow rate (e) nano particle volumetric fraction

Each working fluid would have a different absorbed energy parameter, as shown in Fig. 12. This parameter is the result of heat removal factor, transmittance, and absorbance. The ratio of actual heat transfer to greatest amount of heat transfer that can achieve is represented by the heat removal factor. This parameter has a critical role in determining the amount of useable energy that can be extracted from the collector. For all working fluids taken into consideration as shown in Fig. 12(a),12(b), MgO-TiO_2/water and magnetic particle/water nanofluids are observed to have the best-absorbed energy parameter at 0.1,0.2 % having mean % enhancement is 23 and 24 % followed by clove treated graphene nanoplatelet/water,Al_2O_3/water,Al_2O_3-Fe/water with values 22,18,9 % taking other factors remains constant . At constant temperature as shown in Fig. 12(c),12(d),with increasing mass flow rate the mean % enhancement of absorbed energy parameter for MgO-TiO_2/water, clove treated graphene nanoplatelet/water and magnetic particle/water is highest having value 2 %. this metric rises and stays constant after certain mass flow rate.All the working fluids in this Fig. 12(e) exhibit the impact of the nanoparticle volumetric concentration of absorbed energy parameter.As in this Fig with the increase of nanoparticle volumetric fraction the absorbed energy parameter of MgO-TiO_2/water, clove treated graphene nanoplatelet/water and magnetic particle/water remains constant but there is a decrement in absorbed energy parameter for Al_2O_3/water,Al_2O_3-Fe/water . At 0.05% volumetric fraction this nanofluids shows highest absorbed energy parameter.

6.7 THERMAL EFFICIENCY

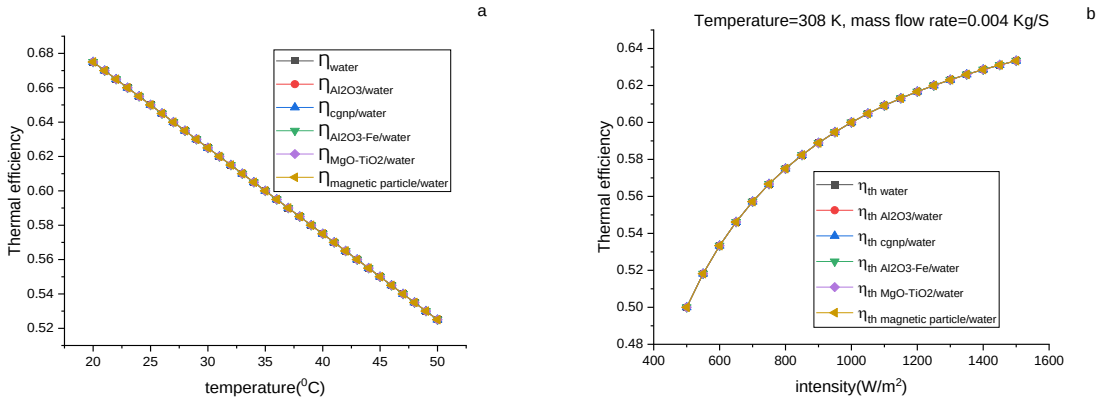

FIG. 13. Thermal efficiency as a function of (a) temperature (b) intensity

The thermal efficiency decreases with the increase in temperature for all working nano fluids taken into account. Since there is an increase in the collector's plate surface temperature would result in more amount of energy being accessible for convective, conductive, and radiative heat losses through collector , this decrease is result of an increase in thermodynamic losses from the absorber plate surface of the collector. Increasing the Reynolds number in the flow zone is one technique to mitigate this loss problem. Increased turbulence and quicker convection losses from the pipe walls to the working nanofluid would result from this. An unexpected result is seen when comparing the nanofluids used in the collection because all nanofluids employed have the same performance as shown in Fig. 13(a). Due to the fact that fluid density and viscosity tend to decrease as temperature rises, thermal efficiency has decreased. Since extremely viscous fluids create a flow resistance, viscosity plays a significant role in fluid flow. Fig. 13(b) depicts the impact of intensity change on collector effectiveness using various nanofluids at nano particle volume concentrations ,constant mass flow rates . With increment of intensity of radiation up to the certain level, all nanofluids show a corresponding gain in efficiency. Beyond that level,

efficiency becomes saturated and stays constant as a result of a corresponding rise in the variety of losses brought on by a greater temperature difference between the absorbing plate and its surroundings. The largest efficiency increase can be shown in Al_2O_3/water, MgO-TiO_2/water, magnetic particle/water, cgnp/water, and Al_2O_3-Fe/water in comparison to water as base fluid for constant mass flow rate at 0.004 kg/s, temperature, and nanoparticle volume concentration.

6.8 EXERGY EFFICIENCY

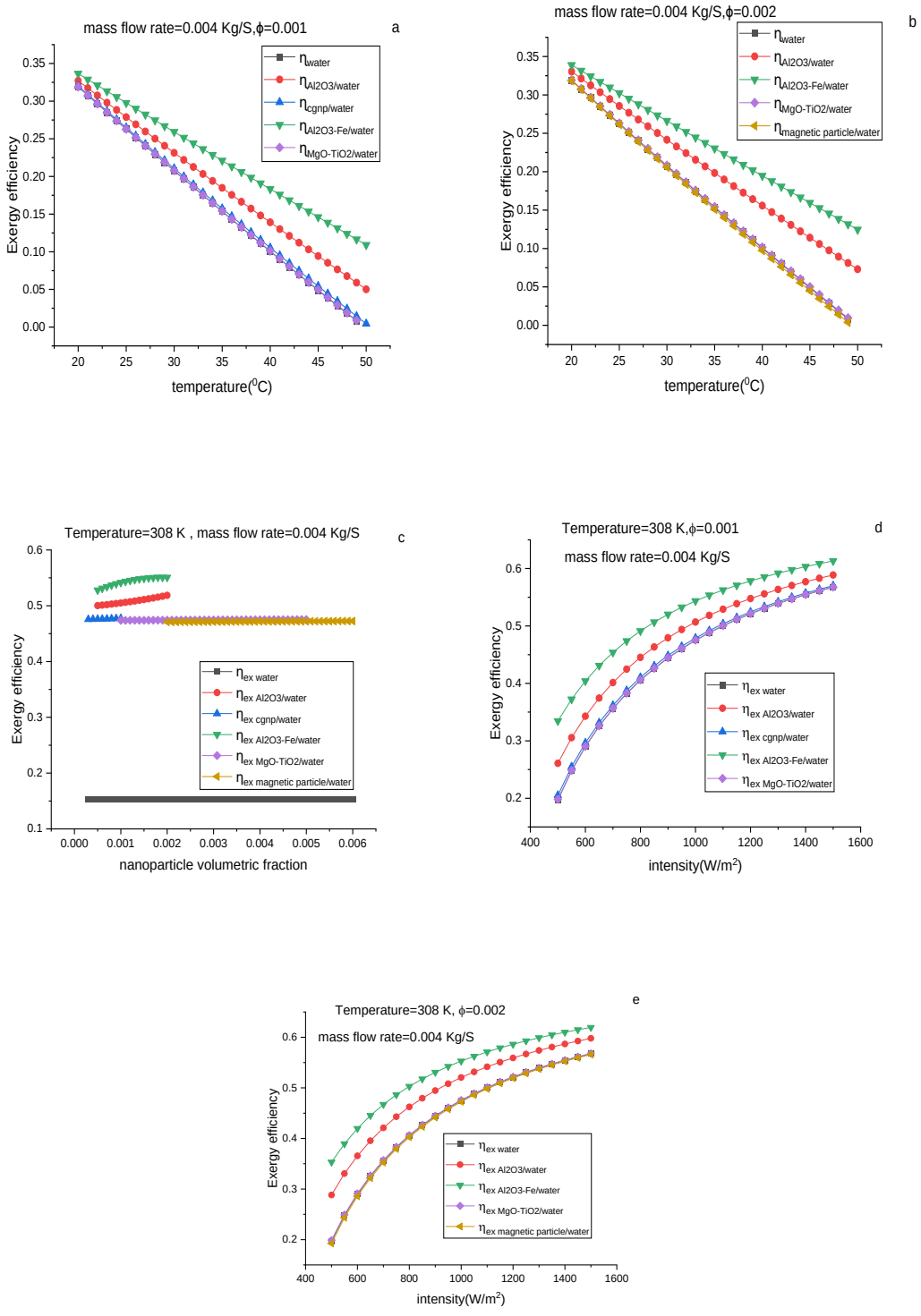

FIG. 14. Exergy efficiency as a function of (a,b) temperature (c) nano particle volumetric fraction (d,e) intensity

Fig. 14(a), 14(b) shows that when the temperature rises, the system's exergy efficiency diminishes. Less heat is available in the system to be transformed into useable energy, which is the cause of this decline. The exergy in the system reduces as a collector's temperature approaches that of the sun because more heat is lost because of heat transfer from the sun to the collector.The utilisation of different types of nanofluids represents a greater exergy performance when compared to the working nanofluids evaluated in this study because of its significantly increased thermal conductivity qualities. With the usage of Al_2O_3-Fe/water nanofluids, exergetic efficiency is typically increased by 27% compared to 14% when using Al_2O_3/water, 0.25 % when using MgO-TiO_2/water nanofluids, and a mean decline of 0.87 % when using cgnp/water and 1.4 % when using magnetic particle/water. Additionally, rising temperature is seen to reduce the increase in thermal conductivity between the nanofluids. The exergetic efficiency of the flat plate collector with varied nanoparticle volumetric concentration is shown in Fig. 14(c). It has been observed that the thermal performance of the collector improves and, for some nanofluids, remains constant as the volumetric proportion of nanoparticles increases. Regarding the utilisation of nanofluids, a rise in concentration would likewise boost the system's performance. The Al_2O_3-Fe/water nanofluid was found to be more effective than other fluids in this investigation for the range of nanoparticles taken into account, with the highest mean performance being observed at a volumetric concentration of 72% of nanoparticles. Fig. 14(d),14(e) illustrates the impact of intensity change on exergy efficiency using various nanofluids at a fixed mass flow rate and nanoparticle volume concentration. With increasing intensity of radiation up to the certain level, all nanofluids show a corresponding gain in efficiency. Beyond that level, exergetic efficiency becomes saturated and stays constant as a result of a corresponding rise in the variety of losses brought on by a greater temperature difference between the absorbing plate and its surroundings. Al_2O_3-Fe/water has the greatest increase in efficiency when compared

to other nanofluids at constant flow rate at 0.004 kg/s, temperature, and nanoparticle volume concentration.

6.9 EXERGY LOSS

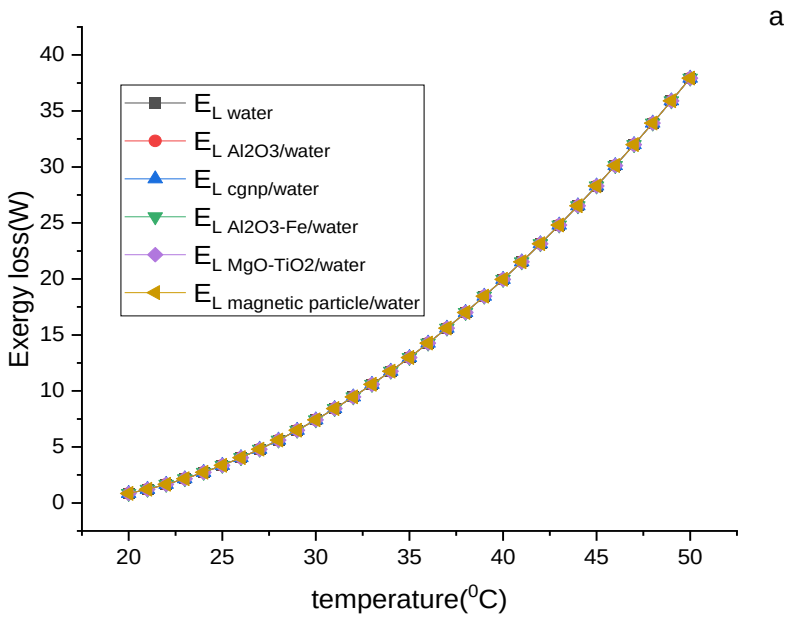

FIG. 15a. Exergy loss as a function of temperature

Fig. 15(a) illustrates how temperature affects the system's energy losses. The losses are shown to increase as the temperature rises, which causes the walls of the collector's absorber to lose heat more quickly. As the value Reynolds number increases, the resistance due to inside the collector shows an decrement, which is why this happens.

6.10 EXERGY DESTRUCTION

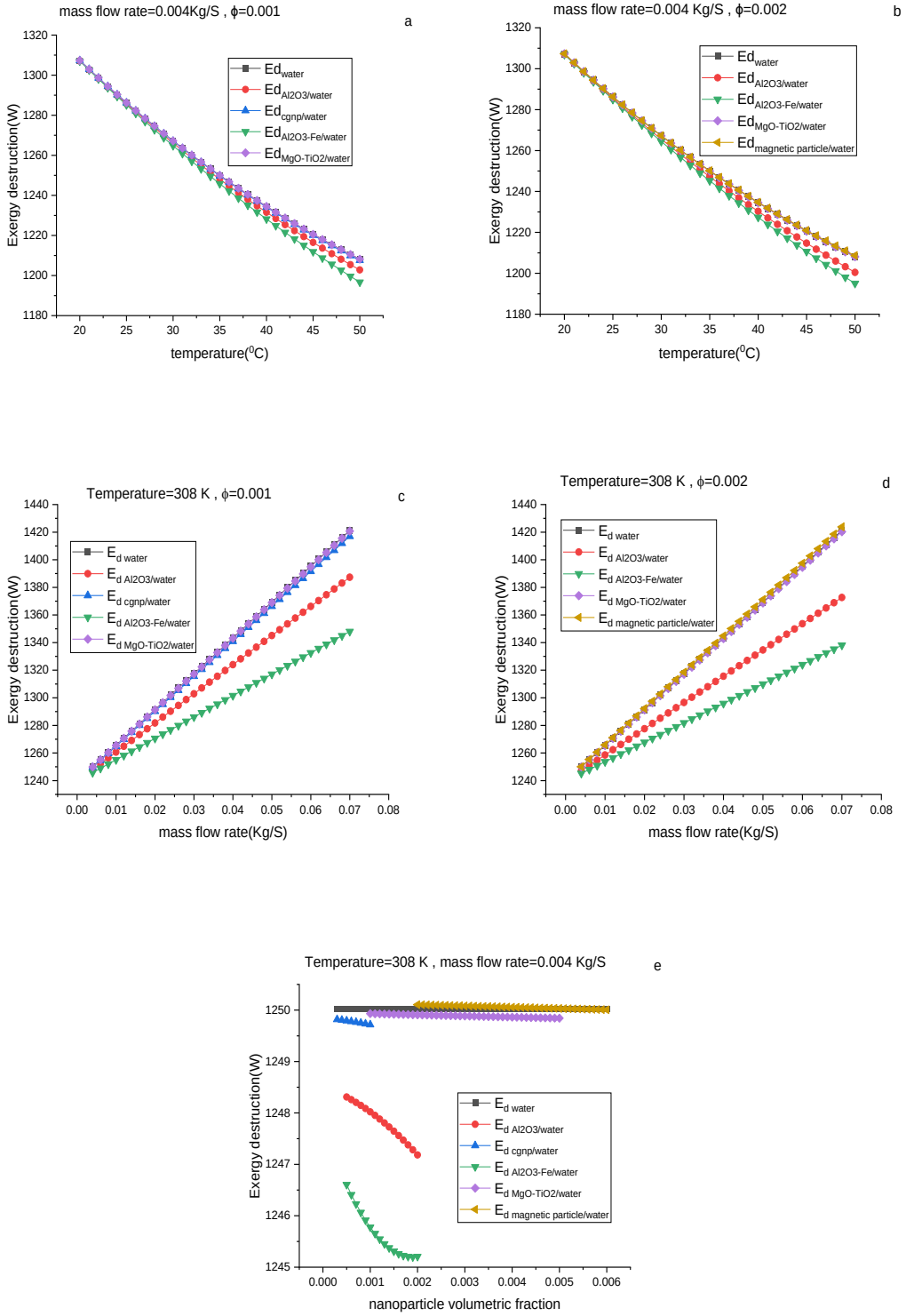

FIG. 16. Exergy destruction as a function of (a,b) temperature (c,d) mass flow rate (e) nano particle volumetric fraction

Fig. 16 displays how each working fluid performs in relation to the distribution of flow of exergy in the solar plate collector. Fig. 16 (a),16(b) shows that the effect of energy destruction in the flat plate collector is reduced by 0.38 % when hybrid Al_2O_3-Fe/water nanofluids are used and then followed by Al_2O_3/water, clove treated graphene nanoplatelet/water, MgO-TiO_2/water and magnetic particle/water nanofluids. The rate of irriversibilities in the system is shown to be decreased by the usage of all nanofluids. This is caused by the nanofluids' enhanced thermal conductivity characteristics. With constant temperature and increasing mass flow rate minimum exergy destruction is for Al_2O_3-Fe/water nanofluid then followed by others as shown in Fig. 16(c),16(d). Similarlarly Fig. 16 (e) shows the effect of the mass flow rate and volumetric fraction on the system's exergy destruction. All the nanofluids have maximum exergy destruction rate initially but as nano particle volumetric concentration increases their exergy destruction decreases. Here in this Fig. 16 (e) magnetic particle/water have highest exergy destruction at 0.2% volumetric fraction and Al_2O_3-Fe/water has minimum exergy destruction.

6.11 ENTROPY GENERATION

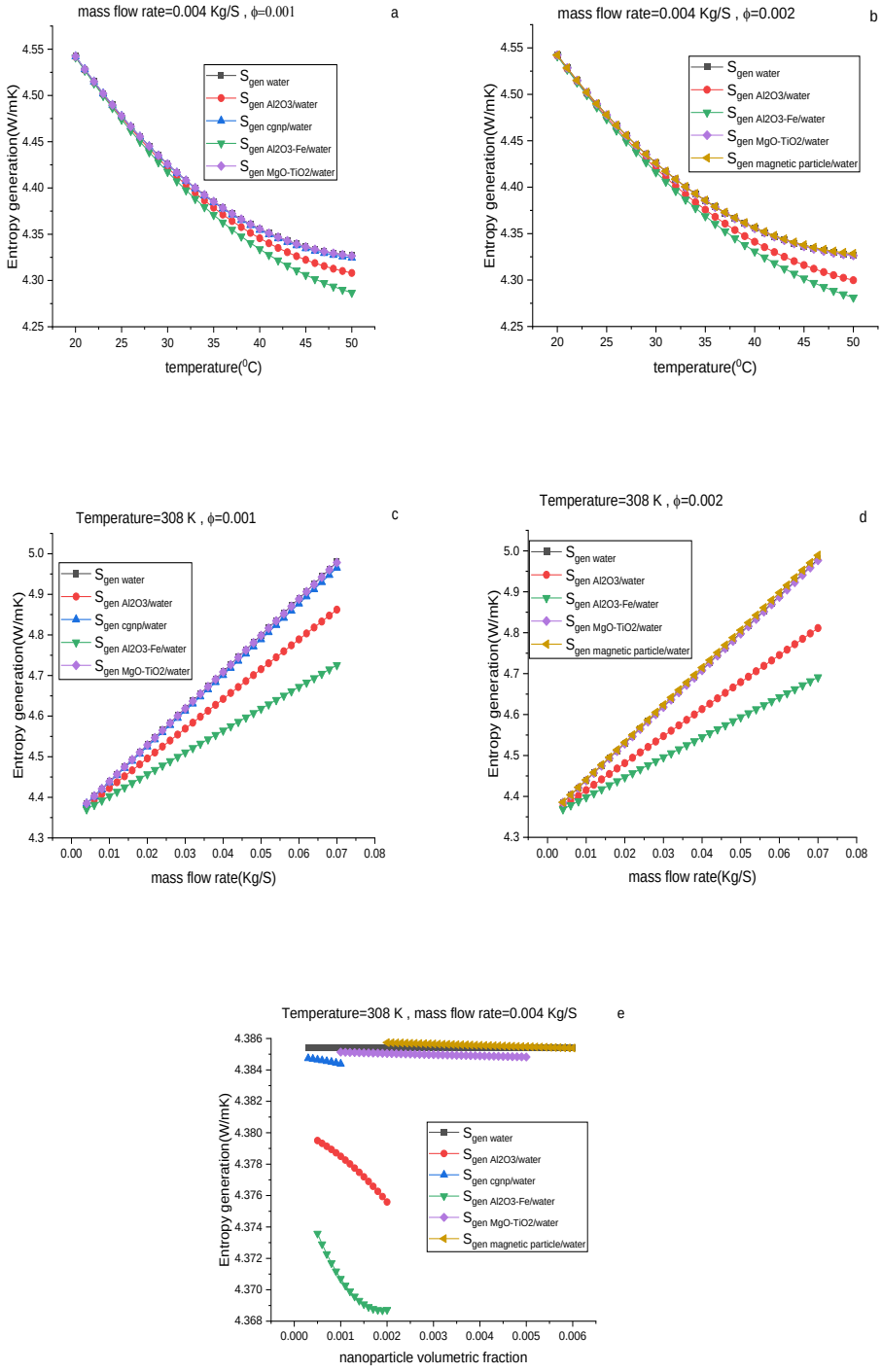

FIG. 17. Entropy generation as a function of (a,b) temperature (c,d) mass flow rate (e) nano particle volumetric fraction

The rate of irreversibilities in a system and its entropy creation are closely correlated. It is calculated by dividing the total of all exergy characteristics by the surrounding temperature. According to Fig. 17(a),17(b) as the collector's temperature rises, the rate of entropy formation reduces in the end it is maximum for MgO-TiO_2/water and magnetic particle/water nanofluids then followed by Al_2O_3/water, clove treated graphene nanoplatelet/water, Al_2O_3-Fe/water. Fig. 16 demonstrates that the heat transfer from the sun to the absorber plate is the source of all energy destruction in the system. This parameter decreases as temperature rises because of the irreversibilities are stronger at lower temperatures due to this features of nanofluids. The irreversibilities brought on by fluid friction decrease as the working nanofluids have less viscosity. Better output temperature is produced by nanofluids at lower mass flow rates, which results in a slower rate of entropy production. Similarly, for magnetic particle/water, MgO-TiO_2/water, and clove treated graphene nanoplatelet/water nanofluids, the largest entropy generation then followed by others, with constant temperature and increasing mass flow rate. All the nanofluids have maximum entropy generation rate initially but as nano particle volumetric concentration increases their entropy generation decreases. Here in this Fig. 17 (e) magnetic particle/water have highest entropy generation at 0.15% volumetric fraction and Al_2O_3-Fe/water has minimum entropy generation.

6.12. BEJAN NUMBER

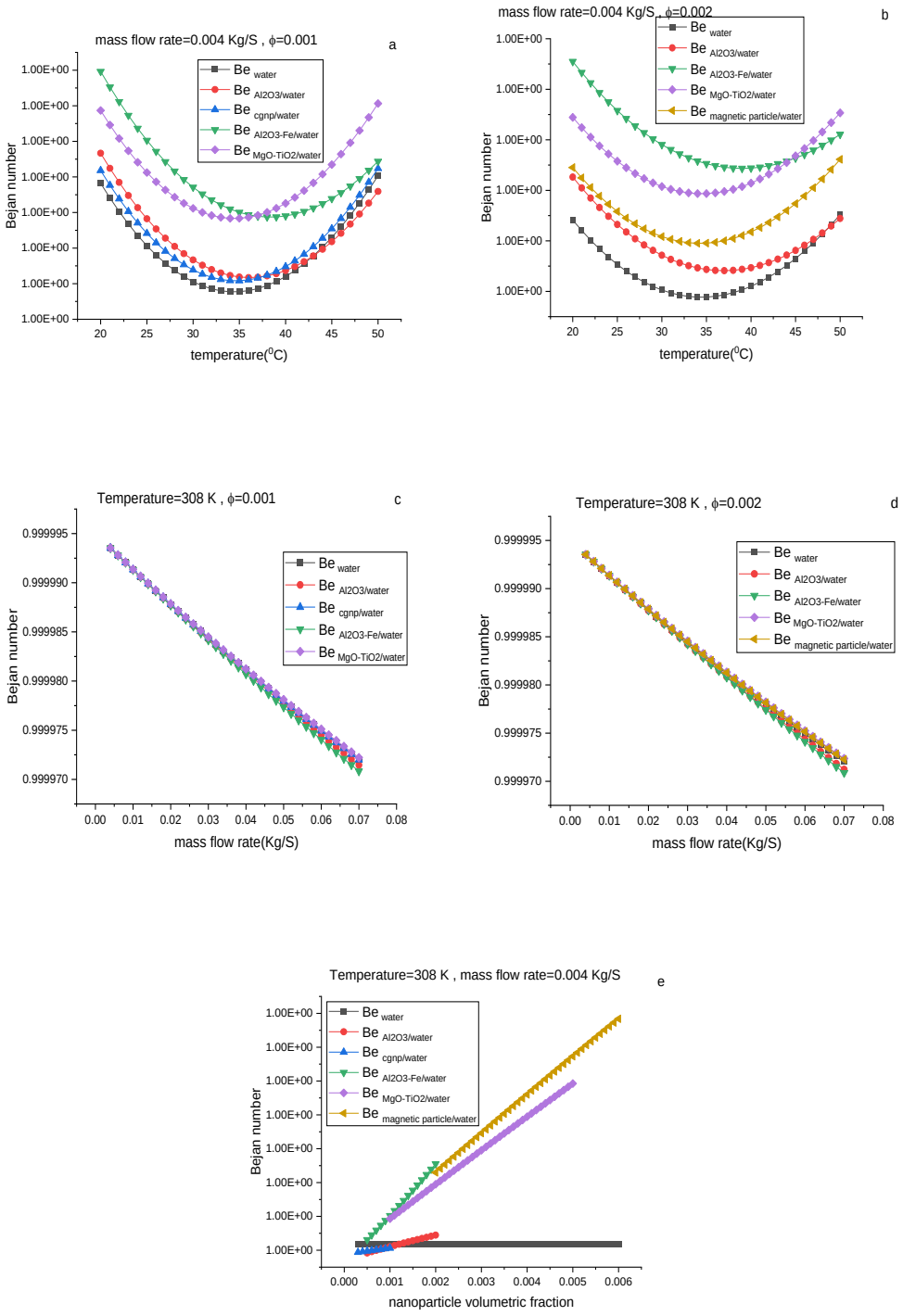

FIG. 18. Bejan number as a function of (a,b) temperature (c,d) mass flow rate (e) nano particle volumetric fraction

The ratio of entropy generated by heat transfer to all other entropy generated in the system is represented by the Bejan number. As a result, the Bejan number's value rises toward one as the amount of energy lost as a result of pressure drop in the system decreases. Fig.18 (a),18(b) shows that when the system's temperature rises, the Bejan number initially falls and subsequently rises closer to 1 as a result of the pressure losses' less pronounced effects at higher temperatures. From a graphical perspective, Al_2O_3-Fe/water initially has the highest value, but MgO-TiO_2/water eventually increases to have the highest value. Fig. 18 (c),18(d) illustrates the opposite, showing that when mass flow rate increases, the Bejan number decreases because pressure drop rises as flow rate increases for all the nanofluids . An increasing trends in bejan number is obtained with the increase of nano particle volumetric fraction keeping all other factors constant as shown in Fig. 18 (e) , magnetic particle/water shows maximum value of Bejan number (closer to 1) at 0.6% volumetric fraction followed by other nanofluids.

6.13 PUMPING POWER LOSS

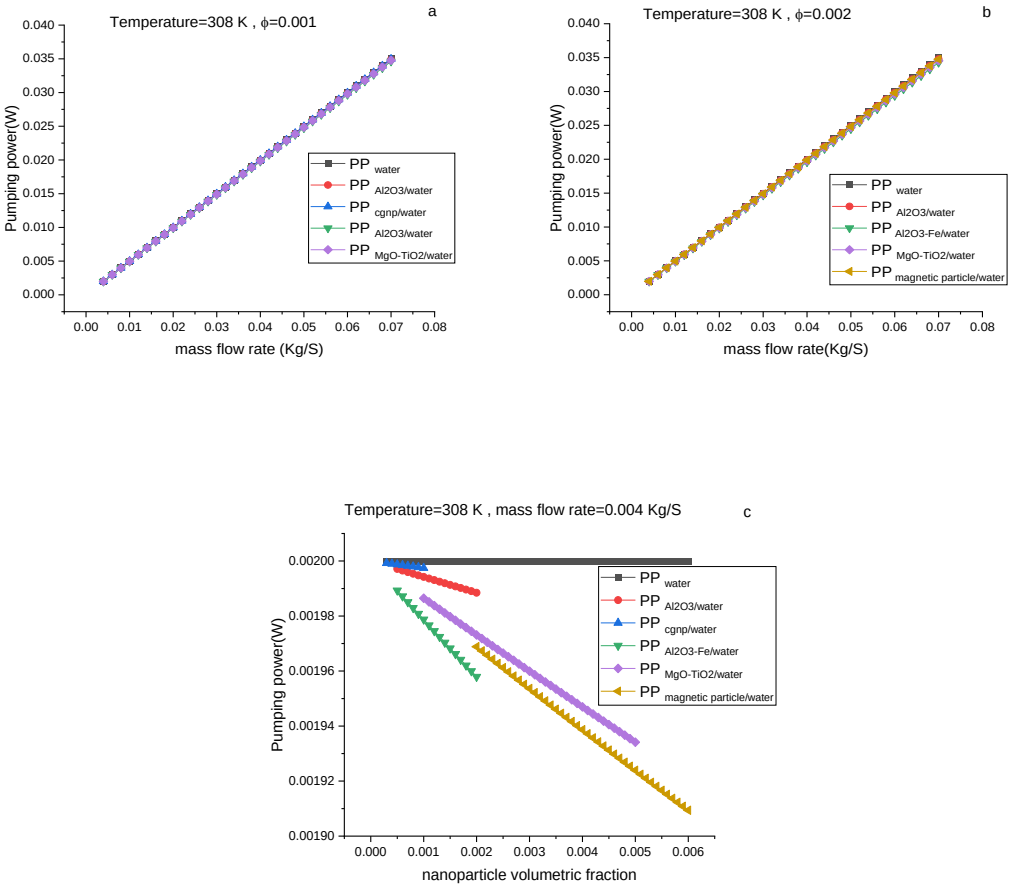

FIG.19. Pumping power loss as a function of (a,b) mass flow rate (c) nano particle volumetric fraction

According to Fig. 19(c), the loss due to pumping power in working nanofluids, which depends on viscosity as well as density, decreases as the nano particle volume concentration increases. According to graphs, magnetic particle/water nanofluid has the lowest pumping power at 0.6% volumetric concentration, which dramatically declines as concentration increases followed by all other nanofluids. For all nanofluids, increasing trends in pumping power are achieved as the mass flow rate of nanofluids increases, as illustrated in Fig. 19 (a),19(b).

7. CONCLUSION

To estimate the successiveness of a flat plate collector using the wide range of nanofluids, a parametric analysis was done. Using water as the basis fluid, various combinations of mass flow rate, temperature, and nanoparticle volumetric %age are assessed. To determine their thermal characteristics throughout a temperature range of 20 to 50 degrees Celsius, theoretical approaches were applied. A polynomial regression model was created from the theoretically generated data for each of the nanofluids' thermal parameters, including thermal conductivity, specific heat capacity, density, and dynamic viscosity.

The outcomes are listed below:

- This study establishes that the viscosity of working nanofluid is a significant factor affecting the thermal performance of flat plate collectors. Al2O3-Fe/water nanofluids do not offer a thermal advantageous working fluid for use in flat plate collectors because of their highest viscosity values among all the nanofluids at the low operating temperatures of the flat plate collector.
- While adding nanoparticles to working fluids improves their performance, a certain volumetric fraction of nanoparticles beyond the level with which adding them to fluid has less impact on the collector's thermal performance.
- Nanofluids significantly increase the heat transfer coefficient in the flow zone. At different temperatures and mass flow rates, MgO-TiO_2/water nanofluids show an improvement in heat transfer coefficient of 89 and 68%, respectively.
- The importance of dimensionless numbers is crucial. The Nusselt number and Reynolds number are all highest for MgO-TiO2/water, and the Prandtl number is the lowest for this nanofluid.

- For the nanofluids under discussion, the friction factor exhibits behavior comparable to viscosity. Al2O3-Fe/water has the highest coefficient of friction at different temperatures and mass flow rates.
- The amount of usable energy that can be recovered from the collector depends on this value. MgO-TiO2/water and magnetic particle/water nanofluids are reported to have the best-absorbed energy parameter for all working fluids.
- All nanofluids exhibit a thermal enhancement in performance in the flat plate collector with an increment in temperature and intensity when there is a concentration of nanoparticles.
- Al_2O_3-Fe/water nanofluids offer a better fluid friction alternative than water, but they also offer a 27 % increase in exegetical efficiency compared to other nanofluids. With the rise of mass flow rate, intensity, volumetric fraction, the exegetic efficiency value for Al_2O_3-Fe/water is higher.
- All nanofluids have an increase in exergy loss as the temperature rises.
- In terms of the exergy flow across the flat plate collector, the exergy destruction because of the temperature difference between the sun and flat plate collector accounted for an average of 38 % of the exergy destruction in Al_2O_3-Fe/water at rising mass flow rates, while the exergy destruction with rising temperature accounts for the minimum source of destruction with 0.01 %.
- As the concentration of nanoparticles in the fluid increases, the rate of entropy formation in the collector decreases due to the increasing thermal conductivity of the nanofluids. Due to a rise in pressure losses in the collector, the system's rate of entropy creation increases as the mass flow rate does. The rate of entropy production decreases as the collector's temperature rises, peaking for MgO-TiO_2/water and magnetic particle/water.

- Because pressure losses have a smaller contribution to exergy destruction parameter, the Bejan number is maximum at lower mass flow rates. Bejan number first lowers as the temperature rises before increasing.
- The pumping power of magnetic particle/water nanofluid is the lowest and dramatically decreases with concentration.

8. FUTURE STUDY

Despite these advantages of nanofluids, several problems still need to be resolved in terms of mass production, stability, cost, and the mechanics of the nanoparticle behavior in the base fluid, among other things. To make the usage of nanofluid a practical and popular alternative, these issues must be resolved. To understand the interaction of nanoparticles with various base fluids, such as ethyl alcohol, vegetable oils, etc., additional research and analysis are required. Future research should focus on using various nanofluids at high-temperature ranges, namely transmitting heat through a base fluid at boiling conditions and their behavior in cryogenic environments.

REFERENCES

1. Lee, S.W., Park, S.D., Kang, S., Bang, I.C. and Kim, J.H., 2011. Investigation of viscosity and thermal conductivity of SiC nanofluids for heat transfer applications. *International Journal of Heat and Mass Transfer*, *54*(1-3), pp.433-438.

2. Kumaresan, V. and Velraj, R., 2012. Experimental investigation of the thermo-physical properties of water–ethylene glycol mixture based CNT nanofluids. *Thermochimica Acta*, *545*, pp.180-186.

3. Nine, M.J., Munkhbayar, B., Rahman, M.S., Chung, H. and Jeong, H., 2013. Highly productive synthesis process of well dispersed Cu2O and Cu/Cu2O nanoparticles and its thermal characterization. *Materials Chemistry and Physics*, *141*(2-3), pp.636-642.

4. Aravind, S.J. and Ramaprabhu, S., 2013. Graphene–multiwalled carbon nanotube-based nanofluids for improved heat dissipation. *Rsc Advances*, *3*(13), pp.4199-4206

5. Nikkam, N., Ghanbarpour, M., Saleemi, M., Haghighi, E.B., Khodabandeh, R., Muhammed, M., Palm, B. and Toprak, M.S., 2014. Experimental investigation on thermo-physical properties of copper/diethylene glycol nanofluids fabricated via microwave-assisted route. *Applied Thermal Engineering*, *65*(1-2), pp.158-165.

6. Elias, M.M., Mahbubul, I.M., Saidur, R., Sohel, M.R., Shahrul, I.M., Khaleduzzaman, S.S. and Sadeghipour, S., 2014. Experimental investigation on the thermo-physical properties of Al2O3 nanoparticles suspended in car radiator coolant. *International Communications in Heat and Mass Transfer*, *54*, pp.48-53.

7. Karimi, A., Afghahi, S.S.S., Shariatmadar, H. and Ashjaee, M., 2014. Experimental investigation on thermal conductivity of MFe2O4 (M= Fe and Co) magnetic nanofluids under influence of magnetic field. *Thermochimica Acta*, *598*, pp.59-67.

8. Li, X., Chen, Y., Mo, S., Jia, L. and Shao, X., 2014. Effect of surface modification on the stability and thermal conductivity of water-based SiO2-coated graphene nanofluid. *Thermochimica acta*, *595*, pp.6-10.

9. Sundar, L.S., Singh, M.K., Bidkin, I. and Sousa, A.C., 2014. Experimental investigations in heat transfer and friction factor of magnetic Ni nanofluid flowing in a tube. *International Journal of Heat and Mass Transfer*, *70*, pp.224-234.

10. Manikandan, S., Shylaja, A. and Rajan, K.S., 2014. Thermo-physical properties of engineered dispersions of nano-sand in propylene glycol. *Colloids and Surfaces A: Physicochemical and Engineering Aspects*, *449*, pp.8-18.

11. Rakhsha, M., Akbaridoust, F., Abbassi, A. and Majid, S.A., 2015. Experimental and numerical investigations of turbulent forced convection flow of nano-fluid in helical coiled tubes at constant surface temperature. *Powder Technology*, *283*, pp.178-189.

12. Huminic, A., Huminic, G., Fleaca, C., Dumitrache, F. and Morjan, I., 2015. Thermal conductivity, viscosity and surface tension of nanofluids based on FeC nanoparticles. *Powder Technology*, *284*, pp.78-84.

13. Yarmand, H., Gharehkhani, S., Ahmadi, G., Shirazi, S.F.S., Baradaran, S., Montazer, E., Zubir, M.N.M., Alehashem, M.S., Kazi, S.N. and Dahari, M., 2015. Graphene nanoplatelets–silver hybrid nanofluids for enhanced heat transfer. *Energy conversion and management*, *100*, pp.419-428.

14. Amiri, A., Sadri, R., Shanbedi, M., Ahmadi, G., Chew, B.T., Kazi, S.N. and Dahari, M., 2015. Performance dependence of thermosyphon on the functionalization approaches: an experimental study on thermo-physical properties of graphene nanoplatelet-based water nanofluids. *Energy conversion and management*, *92*, pp.322-330.

15. Solangi, K.H., Kazi, S.N., Luhur, M.R., Badarudin, A., Amiri, A., Sadri, R., Zubir, M.N.M., Gharehkhani, S. and Teng, K.H., 2015. A comprehensive review of thermo-physical properties and convective heat transfer to nanofluids. *Energy*, *89*, pp.1065-1086.

16. Karimi, A., Sadatlu, M.A.A., Saberi, B., Shariatmadar, H. and Ashjaee, M., 2015. Experimental investigation on thermal conductivity of water based nickel ferrite nanofluids. *Advanced Powder Technology*, *26*(6), pp.1529-1536.

17. Said, Z., Saidur, R., Sabiha, M.A., Rahim, N.A. and Anisur, M.R., 2015. Thermophysical properties of Single Wall Carbon Nanotubes and its effect on exergy efficiency of a flat plate solar collector. *Solar Energy*, *115*, pp.757-769.

18. Azmi, W.H., Hamid, K.A., Mamat, R., Sharma, K.V. and Mohamad, M.S., 2016. Effects of working temperature on thermo-physical properties and forced convection heat transfer of TiO2 nanofluids in water–Ethylene glycol mixture. *Applied Thermal Engineering*, *106*, pp.1190-1199.

19. Sarsam, W.S., Amiri, A., Zubir, M.N.M., Yarmand, H., Kazi, S.N. and Badarudin, A., 2016. Stability and thermophysical properties of water-based nanofluids containing triethanolamine-treated graphene nanoplatelets with different specific surface

areas. *Colloids and Surfaces A: Physicochemical and Engineering Aspects*, *500*, pp.17-31.

20. Maheswaran, R. and Sunil, J., 2016. Effect of nano sized garnet particles dispersion on the viscous behavior of extreme pressure lubricant oil. *Journal of Molecular Liquids*, *223*, pp.643-651.

21. Shanbedi, M., Heris, S.Z., Amiri, A. and Eshghi, H., 2016. Synthesis of water-soluble Fe-decorated multi-walled carbon nanotubes: a study on thermo-physical properties of ferromagnetic nanofluid. *Journal of the Taiwan Institute of Chemical Engineers*, *60*, pp.547-554

22. Li, X., Zou, C., Zhou, L. and Qi, A., 2016. Experimental study on the thermo-physical properties of diathermic oil based SiC nanofluids for high temperature applications. *International Journal of Heat and Mass Transfer*, *97*, pp.631-637.

23. Li, X., Zou, C. and Qi, A., 2016. Experimental study on the thermo-physical properties of car engine coolant (water/ethylene glycol mixture type) based SiC nanofluids. *International Communications in Heat and Mass Transfer*, *77*, pp.159-164.

24. Yarmand, H., Gharehkhani, S., Shirazi, S.F.S., Goodarzi, M., Amiri, A., Sarsam, W.S., Alehashem, M.S., Dahari, M. and Kazi, S.N., 2016. Study of synthesis, stability and thermo-physical properties of graphene nanoplatelet/platinum hybrid nanofluid. *International Communications in Heat and Mass Transfer*, *77*, pp.15-21.

25. Wan, M., Yadav, R.R., Singh, D., Panday, M.S. and Rajendran, V., 2016. Temperature dependent ultrasonic and thermo-physical properties of polyaniline nanofibers reinforced epoxy composites. *Composites Part B: Engineering*, *87*, pp.40-46.

26. Esfe, M.H., Afrand, M., Rostamian, S.H. and Toghraie, D., 2017. Examination of rheological behavior of MWCNTs/ZnO-SAE40 hybrid nano-lubricants under various temperatures and solid volume fractions. *Experimental Thermal and Fluid Science*, *80*, pp.384-390.

27. Gómez-Villarejo, R., Martín, E.I., Navas, J., Sánchez-Coronilla, A., Aguilar, T., Gallardo, J.J., Alcántara, R., De los Santos, D., Carrillo-Berdugo, I. and Fernández-Lorenzo, C., 2017. Ag-based nanofluidic system to enhance heat transfer fluids for concentrating solar power: Nano-level insights. *Applied Energy*, *194*, pp.19-29.

28. Verma, S.K., Tiwari, A.K. and Chauhan, D.S., 2017. Experimental evaluation of flat plate solar collector using nanofluids. *Energy conversion and Management*, *134*, pp.103-115.

29. Zhang, H., Wang, S., Lin, Y., Feng, M. and Wu, Q., 2017. Stability, thermal conductivity, and rheological properties of controlled reduced graphene oxide dispersed nanofluids. *Applied Thermal Engineering*, *119*, pp.132-139.

30. Huminic, G., Huminic, A., Fleaca, C., Dumitrache, F. and Morjan, I., 2017. Thermo-physical properties of water based SiC nanofluids for heat transfer applications. *International Communications in Heat and Mass Transfer*, *84*, pp.94-101.

31. Zawawi, N.N.M., Azmi, W.H., Redhwan, A.A.M., Sharif, M.Z. and Sharma, K.V., 2017. Thermo-physical properties of Al2O3-SiO2/PAG composite nanolubricant for refrigeration system. *international journal of refrigeration*, *80*, pp.1-10.

32. Sadri, R., Hosseini, M., Kazi, S.N., Bagheri, S., Zubir, N., Solangi, K.H., Zaharinie, T. and Badarudin, A., 2017. A bio-based, facile approach for the preparation of covalently functionalized carbon nanotubes aqueous suspensions and their potential as heat transfer fluids. *Journal of colloid and interface science*, *504*, pp.115-123.

33. Nimdeo, Y.M. and Srivastava, A., 2018. Understanding the temperature dependence of thermo-physical properties of nanofluid suspensions using non-intrusive dynamic measurements. *Experimental Thermal and Fluid Science*, *94*, pp.109-121.

34. Sadri, R., Hosseini, M., Kazi, S.N., Bagheri, S., Abdelrazek, A.H., Ahmadi, G., Zubir, N., Ahmad, R. and Abidin, N.I.Z., 2018. A facile, bio-based, novel approach for synthesis of covalently functionalized graphene nanoplatelet nano-coolants toward improved thermo-physical and heat transfer properties. *Journal of colloid and interface science*, *509*, pp.140-152.

35. Sekhar, T.V.R., Nandan, G., Prakash, R. and Muthuraman, M., 2018. Investigations on viscosity and thermal conductivity of cobalt oxide-water nano fluid. *Materials Today: Proceedings*, *5*(2), pp.6176-6182.

36. Esfe, M.H., Zabihi, F., Rostamian, H. and Esfandeh, S., 2018. Experimental investigation and model development of the non-Newtonian behavior of CuO-MWCNT-10w40 hybrid nano-lubricant for lubrication purposes. *Journal of Molecular Liquids*, *249*, pp.677-687.

37. Shi, L., He, Y., Hu, Y. and Wang, X., 2018. Thermophysical properties of Fe3O4@ CNT nanofluid and controllable heat transfer performance under magnetic field. *Energy Conversion and Management*, *177*, pp.249-257.

38. Tadepalli, R., Gadekula, R.K., Reddy, K.V., Goud, S.R., Nayak, S.K., Saini, V. and Dondapati, R.S., 2018. Characterization of Thermophysical properties of Al2O3, TiO2, SiO2, SiC and CuO Nano Particles at Cryogenic Temperatures. *Materials Today: Proceedings*, *5*(14), pp.28454-28461.

39. Yang, L., Mao, M., Huang, J.N. and Ji, W., 2019. Enhancing the thermal conductivity of SAE 50 engine oil by adding zinc oxide nano-powder: an experimental study. *Powder Technology*, *356*, pp.335-341.

40. Ranjbarzadeh, R., Moradikazerouni, A., Bakhtiari, R., Asadi, A. and Afrand, M., 2019. An experimental study on stability and thermal conductivity of water/silica nanofluid: Eco-friendly production of nanoparticles. *Journal of cleaner production*, *206*, pp.1089-1100.

41. Alawi, O.A., Salih, J.M. and Mallah, A.R., 2019. Thermo-physical properties effectiveness on the coefficient of performance of Al2O3/R141b nano-refrigerant. *International Communications in Heat and Mass Transfer*, *103*, pp.54-61.

42. Sulgani, M.T. and Karimipour, A., 2019. Improve the thermal conductivity of 10w40-engine oil at various temperature by addition of Al2O3/Fe2O3 nanoparticles. *Journal of Molecular Liquids*, *283*, pp.660-666.

43. Logesh, K., Tiwari, R., Harish, R. and Ajay, S., 2019. Experimental Studies On Convective Heat Transfer Coefficient of Al203/Ethylene Glycol-Carbon Nano Tube Nanofluids. *Materials Today: Proceedings*, *18*, pp.4738-4744.

44. Ghaffarkhah, A., Bazzi, A., Dijvejin, Z.A., Talebkeikhah, M., Moraveji, M.K. and Agin, F., 2019. Experimental and numerical analysis of rheological characterization

of hybrid nano-lubricants containing COOH-Functionalized MWCNTs and oxide nanoparticles. *International Communications in Heat and Mass Transfer*, *101*, pp.103-115.

45. Karami, H., Papari-Zare, S., Shanbedi, M., Eshghi, H., Dashtbozorg, A., Akbari, A., Mohammadian, E., Heidari, M., Sahin, A.Z. and Teng, C.B., 2019. The thermophysical properties and the stability of nanofluids containing carboxyl-functionalized graphene nano-platelets and multi-walled carbon nanotubes. *International Communications in Heat and Mass Transfer*, *108*, p.104302.

46. Yadav, S.K., Vasu, V. and Paliwal, U.K., 2019. Experimental study on thermo-physical properties of nano-fluids based on copper nanoparticles. *Materials Today: Proceedings*, *18*, pp.525-532.

47. Mahyari, A.A., Karimipour, A. and Afrand, M., 2019. Effects of dispersed added graphene oxide-silicon carbide nanoparticles to present a statistical formulation for the mixture thermal properties. *Physica A: Statistical Mechanics and Its Applications*, *521*, pp.98-112.

48. Huminic, A., Huminic, G., Fleacă, C., Dumitrache, F. and Morjan, I., 2019. Thermo-physical properties of water based lanthanum oxide nanofluid. An experimental study. *Journal of Molecular Liquids*, *287*, p.111013.

49. Yang, L., Ji, W., Zhang, Z. and Jin, X., 2019. Thermal conductivity enhancement of water by adding graphene nano-sheets: consideration of particle loading and temperature effects. *International Communications in Heat and Mass Transfer*, *109*, p.104353.

50. Mousavi, S.M., Esmaeilzadeh, F. and Wang, X.P., 2019. A detailed investigation on the thermo-physical and rheological behavior of MgO/TiO2 aqueous dual hybrid nanofluid. *Journal of Molecular Liquids*, *282*, pp.323-339.

51. Moghadam, I.P., Afrand, M., Hamad, S.M., Barzinjy, A.A. and Talebizadehsardari, P., 2020. Curve-fitting on experimental data for predicting the thermal-conductivity of a new generated hybrid nanofluid of graphene oxide-titanium oxide/water. *Physica A: Statistical Mechanics and its Applications*, *548*, p.122140.

52. Liu, J., Wang, S., Wang, C., Zhao, F., Lei, S., Yi, H. and Guo, J., 2020. Influence of nanomaterial morphology of guar-gum fracturing fluid, physical and mechanical properties. *Carbohydrate Polymers*, *234*, p.115915.

53. Kazemi, I., Sefid, M. and Afrand, M., 2020. Improving the thermal conductivity of water by adding mono & hybrid nano-additives containing graphene and silica: A comparative experimental study. *International Communications in Heat and Mass Transfer*, *116*, p.104648.

54. Arya, H., Sarafraz, M.M., Pourmehran, O. and Arjomandi, M., 2020. Performance index improvement of a double-pipe cooler with MgO/water-ethylene glycol (50: 50) nano-suspension. *Propulsion and Power Research*, *9*(1), pp.75-86.

55. Wang, F., Cao, J., Ling, Z., Zhang, Z. and Fang, X., 2020. Experimental and simulative investigations on a phase change material nano-emulsion-based liquid cooling thermal management system for a lithium-ion battery pack. *Energy*, *207*, p.118215.

56. Hatami, M., Hasanpour, M. and Jing, D., 2020. Recent developments of nanoparticles additives to the consumables liquids in internal combustion engines: Part II: Nano-lubricants. *Journal of Molecular Liquids*, *319*, p.114156.

57. Okonkwo, E.C., Wole-Osho, I., Kavaz, D., Abid, M. and Al-Ansari, T., 2020. Thermodynamic evaluation and optimization of a flat plate collector operating with alumina and iron mono and hybrid nanofluids. *Sustainable Energy Technologies and Assessments*, *37*, p.100636.

58. Wole-Osho, I., Okonkwo, E.C., Kavaz, D. and Abbasoglu, S., 2020. An experimental investigation into the effect of particle mixture ratio on specific heat capacity and dynamic viscosity of Al2O3-ZnO hybrid nanofluids. *Powder Technology*, *363*, pp.699-716.

59. Ranjan, N., Kamaraj, M. and Ramaprabhu, S., 2020. In situ reduction of graphitic oxide by amorphization of magnesium diboride for the superior thermo-optical property based nanofluid applications. *Materials Today Chemistry*, *18*, p.100354.

60. Stalin, P.M.J., Arjunan, T.V., Matheswaran, M.M., Kumar, P.M. and Sadanandam, N., 2021. Investigations on thermal properties of CeO2/water nanofluids for heat transfer applications. *Materials Today: Proceedings*, *47*, pp.6815-6820.

61. Omiddezyani, S., Gharehkhani, S., Yousefi-Asli, V., Khazaee, I., Ashjaee, M., Nayebi, R., Shemirani, F. and Houshfar, E., 2021. Experimental investigation on thermo-physical properties and heat transfer characteristics of green synthesized highly stable CoFe2O4/rGO nanofluid. *Colloids and Surfaces A: Physicochemical and Engineering Aspects*, *610*, p.125923.

62. Tyagi, P.K., Kumar, R. and Said, Z., 2021. Recent advances on the role of nanomaterials for improving the performance of photovoltaic thermal systems: Trends, challenges and prospective. *Nano Energy*, p.106834.

63. Perabathula, S., Teja, N.B., Prasad, P.H.C., Prasad, M.S.C. and Thomas, S., 2021. Performance analysis of mineral oil based nano-lubricants with sulphur impregnated reduced graphene oxide nanosheets. *Materials Today: Proceedings*.

64. O'neill, P., Fischer, L., Revellin, R. and Bonjour, J., 2021. Phase change dispersions: A literature review on their thermo-rheological performance for cooling applications. *Applied Thermal Engineering*, *192*, p.116920.

65. Shi, L., Zhang, S., Arshad, A., Hu, Y., He, Y. and Yan, Y., 2021. Thermo-physical properties prediction of carbon-based magnetic nanofluids based on an artificial neural network. *Renewable and Sustainable Energy Reviews*, *149*, p.111341.

66. Kana, N., Galmed, A., Khamliche, T., Kaviyarasu, K. and Maaza, M., 2021. Thermal conductivity enhancement in MoO3–H2O nano-sheets based nano-fluids. *Materials Today: Proceedings*, *36*, pp.379-382.

67. Li, X., Wang, H. and Luo, B., 2021. The thermophysical properties and enhanced heat transfer performance of SiC-MWCNTs hybrid nanofluids for car radiator system. *Colloids and Surfaces A: Physicochemical and Engineering Aspects*, *612*, p.125968.

68. Zainon, S.N.M. and Azmi, W.H., 2021. Stability and thermo-physical properties of green bio-glycol based TiO2-SiO2 nanofluids. *International Communications in Heat and Mass Transfer*, *126*, p.105402.

69. Nwaokocha, C., Momin, M., Giwa, S., Sharifpur, M., Murshed, S.M.S. and Meyer, J.P., 2022. Experimental investigation of thermo-convection behaviour of aqueous binary nanofluids of MgO-ZnO in a square cavity. *Thermal Science and Engineering Progress*, *28*, p.101057.

70. Singh, S.K., Verma, S.K. and Kumar, R., 2022. Thermal performance and behavior analysis of SiO2, Al2O3 and MgO based nano-enhanced phase-changing materials, latent heat thermal energy storage system. *Journal of Energy Storage*, *48*, p.103977.

71. Lu, B., Zhang, Y., Zhang, J., Zhu, J., Zhao, H. and Wang, Z., 2022. Preparation, optimization and thermal characterization of paraffin/nano-Fe3O4 composite phase change material for solar thermal energy storage. *Journal of Energy Storage*, *46*, p.103928.

72. Ismail, M.F., Azmi, W.H., Mamat, R. and Ab Rahim, R., 2022. Rheological Behaviour and Thermal Conductivity of Polyvinyl Ether Lubricant Modified with SiO2-TiO2 Nanoparticles for Refrigeration System. *International Journal of Refrigeration*.

73. Kalogirou, S.A. (2004) Solar thermal collectors and applications. *Prog. Energy Combust. Sci.*, **30** (3), 231–295.

74. Kalogirou, S. (2009) *Solar Energy Engineering*.

75. ASHRAE Handbook (2009) *Fundermentals (SI Edition)*, American Society of Heating, Refrigerating and Air-Conditioning Engineers Inc., Atlanta, GA.

76. Angayarkanni, S.A., and Philip, J. (2015) Review on thermal properties of nanofluids: Recent developments. *Adv. Colloid Interface Sci.*, **225**, 146–176.

77. Khanafer, K., and Vafai, K. (2011) A critical synthesis of thermophysical characteristics of nanofluids. *Int. J. Heat Mass Transf.*, **54** (19–20), 4410–4428.

78. Okonkwo, E.C., Abid, M., Essien, E.A., Kavaz, D., and Ratlamwala, T.A.H. (2019) Olive Leaf-Synthesized Nanofluids for Solar Parabolic Trough Collector — Thermal Performance Evaluation. *J. Therm. Sci. Eng. Appl.*, **11** (4), 041009 (1–13).

79. Teng, T.P., Hung, Y.H., Teng, T.C., and Chen, J.H. (2011) Performance evaluation on an air-cooled heat exchanger for alumina nanofluid under laminar flow. *Nanoscale Res. Lett.*, **6** (1), 1–11.

80. Incropera, F.P., Bergman, T.L., Lavine, A.S., and DeWitt, D.P. (2011) *Fundamentals of Heat and Mass Transfer*.

81. Okonkwo, E.C., Essien, E.A., Akhayere, E., Abid, M., Kavaz, D., and Ratlamwala, T.A.H. (2018) Thermal performance analysis of a parabolic trough collector using water-based green- synthesized nanofluids. *Sol. Energy*, **170C** (2018), 658–670.

82. Pak, B.C., and Cho, Y.I. (1998) Hydrodynamic and heat transfer study of dispersed fluids with submicron metallic oxide particles. *Exp. Heat Transf.*, **11** (2), 151–170.

83. Sundar, L.S., Singh, M.K. and Sousa, A.C., 2014. Enhanced heat transfer and friction factor of MWCNT–Fe3O4/water hybrid nanofluids. *International Communications in Heat and Mass Transfer*, *52*, pp.73-83.

84. Mostafizur, R.M., Rasul, M.G. and Nabi, M.N., 2021. Energy and Exergy Analyses of a Flat Plate Solar Collector Using Various Nanofluids: An Analytical Approach. *Energies*, *14*(14), p.4305.

85. Struckmann, F., 2008. Analysis of a flat-plate solar collector. *Heat and Mass Transport, Project Report, 2008MVK160*.

86. Duffie, J.A., Beckman, W.A. and Blair, N., 2020. *Solar engineering of thermal processes, photovoltaics and wind*. John Wiley & Sons.

87. Özil, E., and Yaşar, K. (1987) Analysis of Flat Plate Collectors, in *Solar Energy Utilization* (eds.Yuncu, H., Paykoc, E., and Yener, Y.), Springer, Dordrecht, pp. 188–213.

88. Duffie, J.A., and Beckman, W.A. (2013) *Solar Engineering of Thermal Processes Solar Engineering*, John Wiley & Sons, Inc.

89. Mahian, O., Kianifar, A., Sahin, As.Z., and Wongwises (2014) Performance analysis of a minichannel-based solar collector using different nanofluids. *Energy Convers. Manag.*, **88** (2014), 129–138.

90. Kalogirou, S. (2009) *Solar Energy Engineering*.

91. Petela, R. (1964) Exergy of Heat Radiation. *J. Heat Transfer*, **86** (2), 187.

92. Okonkwo, E.C., Abid, M., and Ratlamwala, T.A.H. (2019) A comparative study of heat transfer enhancement in parabolic trough collector based on modified absorber geometry. *J. energy Eng. ASCE*.

93. Okonkwo, E.C., Ratlamwala, T.A.H., and Abid, M. (2019) Energy, exergy, exergoeconomic, and exergoenvironmental study of a parabolic trough collector using a converging-diverging receiver tube. *Int. J. Exergy*, **29** (2/3/4), 131–154.

94. Mahian, O., Kianifar, A., Sahin, A.Z., and Wongwises, S. (2014) Entropy generation during Al2O3/water nanofluid flow in a solar collector: Effects of tube roughness, nanoparticle size, and different thermophysical models. *Int. J. Heat Mass Transf.*, **78** (2014), 64–75.

95. Okonkwo, E.C., Abid, M., Ratlamwala, T.A.H., Abbasoglu, S., and Dagbasi, M. (2018) Optimal analysis of entropy generation and heat transfer in parabolic trough collector using green-synthesized TiO2/water nanofluids. *J. Sol. Energy Eng.*

96. Padilla, R.V., Fontalvo, A., Demirkaya, G., Martinez, A., and Quiroga, A.G. (2014) Exergy analysis of parabolic trough solar receiver. *Appl. Therm. Eng.*, **67** (1–2), 579–586.

97. Okonkwo, E.C., Adun, H., Babatunde, A.A., Abid, M., and Ratlamwala, T.A.H. (2020) Entropy generation minimization in a parabolic trough collector operating with SiO 2 - water nanofluids using genetic algorithm and artificial neural network. *J. Therm. Sci. Eng. Appl.*, **12** (3), 031007 (11 pages).